(4)

INSTITUTE OF THEORETICAL GEOPHYSICS

DEPARTMENT OF EARTH SCIENCES & DEPARTMENT OF APPLIED MATHEMATICS AND THEORETICAL PHYSICS

UNIVERSITY OF CAMBRIDGE

TELEPHONE +44 (0223) 330270
SECRETARY +44 (0223) 333400
TELEFAX +44 (0223) 333450
Telex No: 81240 CAMSPL G
Internet: adam@esc.cam.ac.uk
JANET: adam@uk.ac.cam.esc
Telemail: a.schultz

DOWNING STREET
CAMBRIDGE
CB2 3EQ

Robert J. Silverman
Administrative Contract Officer
Office of Naval Research JD-16
University of Washington
Seattle, WA 98195

10 May 1993

Dear Mr. Silverman,

This letter constitutes a final report for ONR Grant No. N00014-90-J-1254, "BASIC: Beaufort Ambient Seismo-acoustics beneath Ice Cover". Please excuse the delay in getting this to you, as I am presently on leave of absence from the University of Washington, and have had to prepare this report while I am lecturing in England. The report is rather lengthy, as the project funded under N00014-90-J-1254 produced a definitive seafloor seismoacoustic dataset for those carrying out research in long period acoustic noise, as well as earthquake seismology, beneath ice cover. This experiment has wide application to open ocean acoustic research as well, as it explored an extreme, but critical, boundary condition under which coupling of wind stress into the water column, the primary source of open ocean noise, has been nearly eliminated. The data collected under the project will be used in coming years, both alone, and in conjunction with other datasets subsequently collected under ONR funding.

In the event you need to contact me for additional information while I am still on leave of absence, please do so at the phone numbers, or preferably, the e-mail address, in this letterhead.

Yours sincerely,

Adam Schultz

Dr. Adam Schultz

cc: Randall S. Jacobson, Scientific Officer
Director, Naval Research Laboratory
Defense Technical Information Center

Final Report ONR N0014-90-J-1254

Beaufort Ambient Seismo-acoustics beneath Ice Cover

Contents

1. General Overview 2
2. Special Boundary Conditions 3
3. Experimental Overview 3
   3.1 Seafloor Pressure Instruments 3
   3.2 Seismometers 4
4. Previous Work 4
5. BASIC Seafloor Pressure Measurements 5
   5.1 A Model for the Microseismic Spectral Peak 6
   5.2 Interelement Microseismic Coherence 8
   5.3 Very Low Frequency Waves 9
6. BASIC Seismic Measurements 10
   6.1 Teleseisms 11
   6.2 Microseisms 12
   6.3 Comparison Between Onshore and On-Ice Spectral Levels 12
7. BASIC Conclusions 13
8. Refereed Publications and Papers Communicated 14
9. Budget Details 14
10. Literature Cited 14
11. Figure Captions 17
12. Figures

Tables

Table 1. Distant Teleseisms Recorded 11

Table 2. Regional Events Recorded 12

Final Report ONR N00014-90-J-1254

BEAUFORT AMBIENT SEISMO-ACOUSTICS BENEATH ICE COVER (*BASIC*)

Adam Schultz
Brian Lewis

School of Oceanography WB-10
University of Washington
Seattle, WA 98195
(206) 543-5060

Spahr Webb

Marine Physics Laboratory
Scripps Institution of Oceanography A-025
University of California San Diego
La Jolla, CA 92093

1. General Overview

In order to understand the processes controlling ultra low frequency ambient noise within the ocean, it is necessary to vary boundary conditions by examining seafloor noise under different atmospheric and sea conditions. Open ocean with gently sloping continental margin; steeply sloping margin; contrasted basaltic (hard) and sedimented (soft) rock bottom; and ocean entirely covered by sea ice all represent different controls upon noise generation and propagation. By carrying out a coordinated series of array experiments under such different conditions, the physical mechanisms of seafloor ambient noise will be better understood. The BASIC experiment was the second of such coordinated enterprises funded by ONR. The first, a pair of open ocean ventures off the east coast of the US (ECONOMEX/ SAMSON) was carried out by a WHOI/SIO-led consortium and used a variety of instruments including a subset of the new ONR seismometers built by the WHOI/SIO/UW/MIT consortium. The largest such experiment, and third in the series after BASIC, was a UW/SIO consortium to study noise under hard rock and soft rock conditions with environmental controls provided by FLIP (the NOBS experiment carried out in the NE Pacific, which used the entire suite of new ONR instruments). The NOBS analysis is still underway, and a final report will be presented at the conclusion of that project. Information returned from BASIC complements that from NOBS, and the two together provide a comprehensive and integrated view of ocean noise in the very low and ultra low frequency band. In this final report, results are presented from BASIC, which involved deployment of four pressure instruments on the bottom of the Beaufort Sea in March 1990, as well as an on-ice and onshore array of PASSCAL seismometers and REFTEK recorders specially modified for Arctic use.

The seafloor instruments recorded pressure fluctuations in the band from 0.0005 to 8 Hz during a 2-week period. The pressure spectra derived from these measurements show very low energy in the microseism peak near 0.1 Hz in comparison with measurements from the Pacific or Atlantic seafloor. The microseism band shows a series of spectral peaks and valleys likely associated with the modes of the ocean-seafloor Rayleigh wave waveguide. The shape of the microseism peak is remarkably stable during the experiment although the amplitude varies by about 10 dB. The signals are very coherent between adjacent instruments and suggest propagation in the microseism band from a source lying in the azimuth of the Gulf of Alaska to the Norwegian Sea. The pressure spectra rise rapidly toward lower frequency below 0.02 Hz, but Arctic spectra are less energetic than spectra from sites on either Pacific or Atlantic seafloors at all frequencies. The long period energy appears to be related to flexural-gravity waves on the ocean surface. The pressure measurements predict amplitudes for these waves in general agreement with previous tilt and displacement measurements made on the ice.

An array of 1 Hz and 0.2 Hz PASSCAL seismometers was deployed on the ice and onshore at an oil production facility at Deadhorse, near Prudhoe Bay, Alaska. There is convincing evidence for flexural gravity waves at periods near 30 s from on-ice seismometer measurements, also in agreement with the previous tilt studies. Teleseisms from distant earthquakes were recorded onshore; by the seafloor pressure instruments, and in one case atop the ice cover. The quiet sub-ice low frequency environment makes it possible to detect smaller teleseisms than can otherwise be measured on the seafloor. Our success in deploying free-fall autonomous seafloor instruments through the ice (we believe for the first time), and the success in subsequent through-ice recovery, raises the possibility of carrying out systematic Arctic seafloor experiments in future.

2. Special Boundary Conditions

Noise on the seafloor within the frequency range of 0.01 to 50 Hz is understood to be dominated by mechanisms related to the coupling of wind stress onto the sea surface. The nonlinear interaction of oppositely directed sea surface wave trains, originating from interference between primary ocean waves and waves reflected from coastlines, and from changes in wind direction in the middle of storm areas, is known to produce bottom pressure disturbances at twice the frequency of the primary ocean surface waves (*double frequency* or *secondary* microseisms, near 14 seconds period) which couple into the rock waveguide as elastic waves. The steepening and breaking of swell on coastlines is believed to be responsible for the production of smaller *single frequency* or *primary* microseisms (near 7 seconds period, although primary periods longer than 26 seconds have been reported).

Pressure spectra from the seafloor in the Atlantic or the Pacific Ocean invariably show such a pronounced microseism peak between 0.1 and 5 Hz. In the Arctic Ocean, the ice covering the sea surface has a first order effect on the source of much of the ambient noise in the ULF (<1 Hz) band since the ice cover damps the coupling of much of the wind stress from the water column, eliminating these mechanisms as a source of low-frequency sound. A primary motivation in siting this experiment in the Arctic was to search for other sources of low-frequency sound besides the well studied wave-wave interaction mechanism. The shattering of ice during the movement of the ice sheet is also known to be an important intermittent source of sound at frequencies as low as 10 Hz. Ice surface displacement and tilt measurements have detected oscillations of tens of seconds in period that might be detected with a pressure transducer on the deep-sea floor if of sufficiently long wavelength, and also by appropriate on-ice sensors.

The BASIC field program was conducted during the late winter/early spring of 1990 within the Beaufort Sea and on the North Slope of Alaska. The ice covered ocean provided an opportunity to directly decouple local and distant sources of microseismic noise since there were effectively no local nonlinear interactions between opposed surface gravity waves, and hence no source of secondary microseisms. There should have been little steepening and breaking of swell along the coastline, since the Alaskan and Canadian Arctic coast remained largely frozen over. Noise due to nonlinear interactions in the surf zone should have had no local source, and any such noise detected will serve to confirm that such long wavelength surface gravity waves are global, or alternatively, ocean basin-wide, or local in extent.

In addition to examining the partitioning of noise energy between local and distant sources, we have investigated the importance of teleseisms in overall noise levels and spatial coherence.

3. Experimental Overview

Four autonomously recording free-fall Cox-Webb differential pressure gauges (DPGs) were deployed through the polar ice on the bottom of the Beaufort Sea in 3400 m of water. Deployment took place from ice camp APLIS/90, which was a Navy supported site operated under contract by the University of Washington, a small part of which was supported by funds made available through this contract (N00014-90-J-1254). A polar regional map showing the approximate mean location of APLIS/90 and the location of Prudhoe Bay is seen in Figure 1.

3.1 Seafloor Pressure Instruments

The instruments are designated by color: red, white, green, and blue. The instruments were deployed through the same hole over a 4-h period on 16 March 1990. The ice sheet during this interval was drifting at a rate of nearly 500 m/h. During the 3-week course of the experiment, the ice camp drifted in a large loop ending up about 15 km from the deployment site. For a time, the camp was over 30 km from the deployment site. The trajectory of the ice station, seen in Figure 2, determined the locations of the instruments on the bottom, seen in Figure 3. The direction of station drift changed slightly during the deployments. The instruments lie along a roughly 1.5 km long, gently curving arc with interelement spacing of about 500 m. The instruments were acoustically tracked during and after deployment using a long baseline acoustic array maintained by the Applied Physics Laboratory of the University of Washington. The relative instrument locations are known to better than a few meters. The positions were tied into geodetic coordinates using GPS, and absolute locations are known to better than 100 m. We had originally planned to deploy a 2D array, but the very fast drift of the ice during this period required greater synchronaeity of the deployments than was thought possible at multiple remote sites.

The four instruments were designed for helicopter transport under difficult conditions, and to fit easily through a 1-m-diam hole melted through the ice (Figure 4). The pressure fluctuations were detected using a differential pressure gauge which has lower noise compared to conventional low-frequency hydrophones at frequencies below 0.1 Hz, although poorer performance above 1 Hz.

The self-buoyant instruments were released from their anchors by acoustic command on 5 April 1990. After rising

to the ice cover, the instruments moved with the floe after release and were suspended 30 m below the ice by the flotation. This was arranged to give the transponder within each EG&G 8242 acoustic release a clear line-of-sight path to a hydrophone suspended through the ice, despite deep ice keels between the hydrophone and the instruments.

The instruments were located using several measurements of bearing and distance in successive approximations carried out using a specially modified EG&G deck unit equipped, under this contract, with a short baseline bearing-sensitive transducer array. Two helicopters and crews were contracted for from NOAA, and enabled us to rapidly drill holes in the ice, drop the deck unit transducer through the hole, and take range and bearing measurements. Some ambiguous measurements were generated by reflections from nearby ice keels, but all the instruments were located within a 2-day period, at which time radio beacons were left in place to mark the instrument locations below the ice. Four 1-m-diam holes were melted through the ice using a UW/APL thermal generator and pumping unit transported to each site by helicopter, and divers were able to quickly locate each instrument. The instruments were retrieved and flown back to camp on 7 April 1990. The timing was then checked against time maintained by a rubidium clock, and the tapes retrieved from the instruments. Three of the four instruments obtained complete records, the fourth ("white") stopped recording after 2 days.

An 8088 microcomputer controlled the acquisition of data and drove the small (40 Mbyte) cartridge tape recorder used for recording. The instruments recorded pressure fluctuations sampled continuously at a 16-Hz rate. Tape capacity was sufficient for a 14-day record at this rate. Timing was maintained by a temperature compensated quartz clock. The clock drift at the end of the record was precisely measured, and timing after correcting for drift is thought to be better than 20 ms over the 3-week period, with the exception of the instrument "red" because of the discovery of a 364 ms jump in the rubidium clock time standard used to start the instruments.

The seafloor instruments collected a continuous record of pressure fluctuations during the first 14 days of the experiment. Because of the very quiet low frequency Arctic seafloor conditions, the measurements proved to be sensor noise limited above 2 Hz. As far we know this is the first long record of low-frequency noise obtained on the Arctic seafloor.

3.2 Seismometers

Two sets of 3 component 1 Hz PASSCAL seismometers (Teledyne, Model S13, both vertical and horizontal) and one set of 3 component 0.2 Hz seismometers (Kinemetrics SH-1 and SV-1) were installed at two locations on the surface of the large ice floe on which APLIS/90 was situated. "Vault 1" which contained both 1 Hz and 0.2 Hz three component seismometers, was located approximately 1.8 km distant from APLIS/90. A backup site, "Vault 2", containing only 1 Hz instruments, was located about 300 m from APLIS/90. Vault 1 operated perfectly, although the extreme temperature degraded the performance of the vertical 0.2 Hz component. Vault 2 experienced a hardware failure, with a sticky mechanical relay putting this instrument in calibration mode for the duration of the experiment. An additional set of 1 Hz seismometers were installed at an Arco oil production facility onshore near Prudhoe Bay, at Deadhorse, Alaska ("Vault 3"). This station operated flawlessly, and was used to monitor the component of the microseism wave field that propagates onto the continents.

REFTEK Model 72A dataloggers were used to record the seismic data. The seismometers sampled continuously at 1 kHz on each channel, and after digital FIR filtration, the 21-bit resolution data were stored as 8-Hz samples. All seismometers were synchronized against an Omega time standard. We designed elaborate packaging with extremely thick foam insulation and small ohmic heaters to enable the REFTEK hard disks to operate at external temperatures which at times fell below -40°C. Banks of ten 2000 A-h Edison Carbonaire batteries provided the substantial power requirements for these systems. The REFTEK units, seismometers, and support equipment were provided by the PASSCAL Instrument Center at Lamont.

We have also assembled a seismic dataset from the station at College, Alaska for the period of our observations, with the intent of using this to refine the microseismic beam forming carried out under this project.

4. Previous Work

Milne et al. describe measurements of ambient noise at frequencies as low as 20 Hz from hydrophones towed across the Beaufort seafloor in 451 m of water. These measurements showed great variability in the noise levels near 20 Hz, but demonstrated that very low noise levels could be found at Arctic seafloor sites. Measurements at longer periods in the Arctic have been mostly restricted to measurements from hydrophones suspended from the ice. The pressure signal associated with low- frequency sound is greatly reduced at depths much less than one-half of a wavelength because of

reflection at the free surface, and therefore suspended hydrophones are probably useless for the study of sound below a few Hz. Measurements obtained with hydrophones in midwater at low frequencies are dominated by flow noise and cable strum. Lewis and Denner (1987, 1988) deployed an extensive array of drifting buoys to map acoustic signal levels in the Beaufort Sea. They report an inertial period fluctuation in acoustic levels at 3.2 and 10 Hz, indicative of flow and strum noise. This problem was most severe during the summer months when the rate of drift was the fastest. Data from the winter months were less affected by flow noise. Their study provides the most complete record of long-term variability and spatial coherence of low-frequency sound in the Beaufort Sea.

We found only one example in the literature of seismic instruments deployed on the Arctic ocean floor to study signals below 1 Hz (Prentiss and Ewing, 1963). Very low signal levels were found in the band from 0.1 to 1 Hz in short records obtained from three sites on the seafloor using an ocean bottom seismometer system tethered to the ice surface. Instrument noise predominated at lower frequencies. Only about 2.5 h of records were obtained during this experiment, but from these results the authors concluded the Arctic ocean floor was a very quiet location from which to record signals from distant earthquakes.

At the seafloor in either the Atlantic and Pacific ocean, the pressure spectrum is relatively energetic at frequencies below 0.03 Hz. Low frequency ocean waves (infragravity waves) at these frequencies are of sufficiently long wavelength and energetic to overwhelm other sources of low-frequency pressure fluctuations. Infragravity waves may be generated at coastlines by a conversion through nonlinear processes from short period wave energy (wind driven waves or swell) into long period waves (Webb et al, 1991). Since no waves break on Arctic shores in winter, one would expect this source of low-frequency pressure fluctuations to be absent in the Arctic. However, several groups of researchers have deployed long period seismometers (or gravimeters) on the Arctic ice and detected oscillations primarily in the band from 0.017 to 0.05 Hz (periods from 20-60 s) (LeSchack and Haubrich, 1964; Crary et al, 1952; Hunkins, 1962). These motions are also detected on strain gauges and tiltmeters deployed on the ice (Czipott and Podney, 1989; Williams et al, 1989). These distortions of the ice are either driven by the local wind, or propagate in from the open ocean. Some evidence of wavelike propagation has been seen in the on-ice measurements.

5. BASIC Seafloor Pressure Measurements

The seafloor pressure component of BASIC was the core of the project, and its description will constitute the bulk of this report. A typical raw record of ambient seafloor pressure observations, during a time period free from teleseisms, is seen in Figure 5. A power spectral density plot corrected for instrument response, for a record spanning 12 hours is seen in Figure 6. Strong peaks are evident at periods centered near 13 s, 6.625 s, 3.33 s, 1.92 s and higher multiples. Models of Rayleigh wave propagation will be used later in the discussion of these spectral peaks, which are obviously associated with single and double frequency microseisms. More immediately, a comparison must be made with the Beaufort Sea spectrum and spectra from open oceans. The floor of the Beaufort Sea is very unenergetic in comparison to measurements from any site in the eastern Pacific or the western Atlantic Ocean (Figure 7). The microseism band peaks are very small compared with open ocean peaks, and a slight shift in frequency is apparent. There is a sharp rise toward very low frequency apparently associated with infragravity waves, but the energy at these frequencies is also much less than at any site on the Pacific seafloor. The low signal levels at this site reveal the electronic noise limit of the differential pressure gauges near 10^{-2} Pa^2/Hz at 0.5 Hz and 10^3 Pa^2/Hz above 1 Hz for the best instrument (Figure 7). The spectra from the four instruments look virtually identical, and the data is coherent at all frequencies for which the signal level is above the noise (Figure 8).

The relatively high noise level in the differential pressure gauges was surprising, and made it difficult to detect energetic ice-cracking related events at frequencies above 1 Hz. Buck and Wilson (1986) have reported ice cracking related noise levels near an ice ridge of 10^2 Pa^2/Hz at 10 Hz during noisy intervals. Lewis and Denner (1987, 1988) also report noise levels at 10 Hz detected with drifting buoys as high as 10^2 Pa^2/Hz during some intervals in the winter. Makris and Dyer (1986) report a broad peak around 15 Hz reaching 10^{-3} Pa^2/Hz associated with ice cracking. Typical levels near 10 Hz during quiet intervals have been reported to be near 10^5 Pa^2/Hz (Kutschale, 1969). No such events of sufficient energy to rise above the high frequency DPG noise floor were seen in the present experiment.

In Figures 6 through 8, we see a primary frequency microseism peak near 0.08 Hz, and a double frequency microseism peak that is further divided into a series of peaks near 0.15, 0.31, 0.54, 0.73, 0.95, and 1.16 Hz (there is a slight frequency shift between the peaks in the various figures since they are for spectra from different time periods). The single frequency microseism peak is associated with Rayleigh waves energized by the pounding of ocean waves

along the world's coastlines (Hasselmann, 1963). The double frequency microseisms are created by nonlinear interaction of ocean waves in the open ocean and near the coasts.

The amplitude and shape of the microseism peak is remarkably stable over the duration of the experiment (Figure 9). Measurements of the microseism energy from sites in the Pacific or the Atlantic vary from day to day by as much as 30 dB as the ocean wave climate varies. In contrast, the Arctic measurements show only about a 10-dB variation in the energy in the microseism peak during the experiment with the exception of an interval affected by wave trains from two large earthquakes (Figure 10). The energy varies on time scales on the order of a few days, which is typical of ocean storms. At other sites, the microseism spectrum varies in concert with changes in the local ocean wave spectrum, but there is persistent low-frequency component of the microseism wave field associated with distant storms over the ocean (Webb and Cox, 1986; Kibblewhite and Ewans, 1985). The ocean wave field evolves toward lower frequency and larger waves under a persistent wind. The spectrum of the swell may shift with time toward shorter period and smaller waves as a consequence of dispersion (waves from distant storm sources). These types of evolution of the wave field are often apparent in the seafloor microseism spectra as well, with slow shifts in frequency of peaks in the microseism spectra on the time scale of a few days. In contrast, no long term shifts in the frequency of individual peaks are evident in the Arctic data. The Arctic microseism signal is probably "teleseismic" and caused by ocean waves over a broad area of the world's oceans. The day to day variability of the ocean wave field may be obscured by averaging over a large area. The multiple peaks in the spectrum appear unrelated to the ocean wave spectrum.

Occasional, large earthquakes generate long-lived wave trains that are very apparent in the spectral record as large peaks centered around a 25-s period (Figures 9 and 10). The most prominent event is a sequence of two earthquakes (M_s = 5.5 and M_s = 6.9) near Costa Rica on 25 March 1990. This event occurs in the interval near 192 h in Figures 9 and 10. The seafloor measurements are dominated by the Rayleigh surface wave component. In contrast, the measurements of Keenan and Dyer, using near surface hydrophones under the ice show primarily the water borne "T" phase component.

5.1 A Model for the Microseismic Spectral Peak

The series of evenly spaced troughs and peaks across the microseism peak in the Arctic measurements must be related to the modes of propagation in the ocean-rock waveguide of the Arctic ocean. The simplest model of an ocean waveguide with a pressure release surface and a reflecting bottom leads to a series of modes existing within a frequency range bounded below by the frequencies:

$$f_n = (n + \frac{1}{2})\,(\frac{c}{2h}); \qquad n = 0, 1, 2, \ldots$$

where h is the water depth and c is the speed of sound (Figure 11). These are the quarter wave and higher resonances of the waveguide. The water depth (h) at the Beaufort site is 3400 m, so the cutoff frequencies are at 0.11, 0.33, 0.55, 0.77 Hz, etc. The relationship between these frequencies and the peaks in the seafloor pressure spectrum seems apparent. In this model, the group velocity of each mode approaches zero near the cutoff frequency. A simple model of modes propagating in water of varying depth would require peaks in the spectrum associated with minimums in the group velocity to maintain a constant energy transport.

The modal structure becomes very complex in a more realistic ocean model. The structure of the Beaufort seafloor includes from 4 to 8 km of sediment (Kennett, 1990). The soft sediment profoundly affects the character of the modes of the oceanic waveguide (Panza, 1985). Figure 11 displays the phase velocities of the first 20 Rayleigh modes in a model for this site in the Beaufort Sea. The phase velocity curves for the first four modes in the rigid seafloor model are shown dashed. At these low frequencies there are no distinct ocean waveguide acoustic modes; rather the ocean is just part of a much larger waveguide involving the ocean, sediments, and rocks of the crust and upper mantle. The density of modes at acoustic velocities near 1.5 km/s is increased threefold by the presence of the deep sediment layer in comparison to the rigid seafloor model. At these low frequencies the usual ocean waveguide associated with the ocean sound velocity minimum is unimportant. The ocean, sediments, and mantle rocks have very different compressional and shear velocities so that each acts like a waveguide with a characteristic mode type. This concept is only approximate and a real mode in this complicated set of waveguides will involve energy propagating in all layers. Figure 11 shows evidence for these three interconnected waveguides. Rayleigh modes propagate at mantle shear velocities (3.5 + km/s), and generate displacements at great depth. The ocean and seafloor form the second waveguide; modes

propagate essentially as acoustic waves in the ocean (1.5-3.5 km/s). The third set of modes propagate as shear modes in the sediments (<1.5 km/s). These three types of waves merge together into a single set of dispersion curves. The character of each mode may change abruptly with small changes in frequency along the dispersion curve.

Previous work on mode propagation on the seafloor has suggested that often the energy at any particular frequency in the microseism peak will be associated almost exclusively with a single mode. There is usually only a narrow band of frequencies for which a mode will propagate at phase velocities between 1.5 and 3 km/s. Microseisms are excited by processes at the ocean surface. The eigenfunctions of the faster modes are largest at deeper depths, and are more weakly excited than slower traveling components (Webb and Cox, 1986; Schreiner and Dorman, 1990). Waves traveling at speeds less than the speed of sound in water (1.5 km/s) have eigenfunctions that are evanescent from the seafloor in both directions. The slowest modes are weakly excited by sources at the sea surface and also experience significant dissipation because of the localization of energy within the sediment layer. These "Stoneley" modes may be generated by scattering at the rough rock-sediment boundary and so become an important component of seafloor noise, but the evidence is inconclusive (Schreiner and Dorman, 1990). At the Arctic seafloor site scattering processes are probably insignificant because of the great depth of the sediments. In shallow (shelf depths) water the Stoneley modes are directly excited by the surface sources and dominate the microseism spectrum (Schmidt and Kuperman, 1988).

The phase velocity curves for the modes in the Beaufort Sea model are approximately coincident to the rigid seafloor model phase velocity curves at some frequencies at phase velocities near the speed of sound in water (1.5 km/s). Chiaruttini et al (1985) have shown that the eigenfunctions for the modes in a complex (more complete) model will resemble the eigenfunctions derived from a simpler model in frequency bands for which the phase velocity curves for the two models are nearly coincident (Chiaruttini et al, 1985). In the frequency band from 0.1 to 0.2 Hz, the eigenfunction for the third mode in the realistic ocean model should resemble the eigenfunction for the simple rigid seafloor model, with most of the energy associated with acoustic energy in the ocean (Figure 12). This resemblance is limited to the band in which the phase velocity curves coincide; the eigenfunctions are very different at frequencies outside of the band. We suggest these "pseudoacoustic" modes are associated with the regular sequence of peaks and troughs in the Arctic seafloor pressure spectra.

One hypothesis is that the peaks in the Arctic spectrum are associated with the reflection and transmission of, or coupling between Rayleigh modes at the continental shelf. This problem has been extensively studied, but only at frequencies below the microseism peak (Drake and Bolt, 1989). It may be feasible to calculate coupling coefficients for down slope propagation of Rayleigh waves (Kennett, 1990). The mode coupling problem in the purely acoustic case is still complicated (Kuperman et al, 1991). We have collected seismic data at a station in Prudhoe Bay, Alaska, south of the deployment site and continue to study this record of microseisms in comparison with the seafloor measurements to look at the transmission of microseisms across the shelf.

A second hypothesis, as suggested earlier, is that the peaks in the spectrum are associated with maintaining a constant energy flux as the group velocity and eigenfunction of each mode varies during propagation downslope (adiabatic modes). To examine these two possibilities we use a simple model of a source at the shelf edge (modeling the elastic wave energy propagating across Alaska) and propagate the signal down slope to the site. The model is 2D, with no variation along shore. One set of calculations uses an ocean of constant depth (3.4 km). The ocean floor just beyond the continental shelf north of Alaska lies at a depth of about 2.5 km. A second set of calculations starts the modes at 2.5-km depth and propagates the modes adiabatically to the site at 3.4-km depth.

The first problem is to model the excitation of the modes at the shelf edge. A Rayleigh wave in a half-space has an eigenfunction that decays away from the free surface exponentially. The wave number and frequency spectra of microseisms measured midcontinent with the LASA array show most of the energy is in the fundamental mode Rayleigh wave at long period and in higher-order modes at frequencies between 0.2 and 0.3 Hz, and in compressional waves at higher frequencies (Lacoss, 1969). We model the fundamental mode incident at the shelf edge as a displacement of a vertical wall in the ocean layer. The displacement decays exponentially with depth with an e-folding distance equal to 3.5 km/s divided by the radian frequency. This velocity is characteristic of fundamental and higher modes on land in this frequency band. A simpler source model (a vertical line force at the sea surface) generated similar results. The frequency spectrum of the source is assumed to be white (constant in frequency), and the third dimension parallel to the coast is established by extending the source to infinity in the direction along the coast (no dependence in the alongshore direction).

We use a Green's function technique to determine the excitation of modes. Following Aki and Richards (1980), the pressure signal at the seafloor at a point (x_O, z_O) due to a point force of amplitude f at (x,z) with harmonic time depen-

dence can be written as a sum over the mode Green's functions:

$$p(x_0, z_0, t) = fe^{i\omega t}\sum_n G_n(x_0, z_0; x, z; \omega);$$

for a horizontal point force:

$$G = [(u(z)p(z_0))/(4\omega U I_1)]J_0(k|x_0 - x|),$$

where u and p are the horizontal displacement and pressure field associated with each mode. The group velocity is U. I_1 is an integral over depth of the density weighted sum of the squares of the displacements and proportional to the kinetic energy density in each mode. We model the Rayleigh waves propagating across Alaska from the Pacific ocean associated with this distant microseism source as a line source along a vertical wall representing the shelf edge. The pressure signal at a distance away from the coast can be predicted by integrating in depth the product of the Green's function with a model of the vertical dependence of the source, in this case an exponential function with a characteristic scale.

The second part of the problem is to model the changing mode amplitudes as the waves propagate from near the shelf into deeper water offshore. Here, we use adiabatic mode propagation arguments. The amplitude of the modes is adjusted to maintain constant energy transport from shallow to deep water, and the mode eigenfunction is reevaluated at the water depth appropriate for the receiver location. We assume the phase between modes becomes random some small distance from the coast so that the power in each mode can be added together to determine the pressure spectrum at the receiver.

Figure 13 shows the results of these calculations. The remarkable resemblance of the model spectrum to the measured spectrum despite no frequency dependence of the source demonstrates the importance of modes in determining the spectral shape. The amplitude of the single frequency peak at 0.08 Hz is much too large compared to the amplitude of the double frequency microseisms at 0.11 Hz, but otherwise the predicted amplitudes for the various peaks appear correct. The single frequency energy detected at continental sites is usually 20 to 30 dB smaller than the double frequency peak since the mechanism creating the single frequency peak is very different from the double frequency mechanism. The shear modulus of the near surface sediments is important in determining the amplitude of the peaks and troughs in the spectrum; the peaks disappear if the shear modulus is very small. The pseudoacoustic modes should look more like acoustic modes over a rigid bottom when the seafloor is more rigid. This result is in agreement with the view that the pseudoacoustic modes are associated with the periodicities in the spectrum. The locations of the peaks in the model fit the observations only poorly, but the character of the spectrum is well modeled. This component of the modeling suggests that it is the coupling of the energy at the shelf break into waveguide modes that determines the shape of the spectrum.

The fit can be greatly improved by changing the water depth in the model, perhaps accounting for changes in the mode amplitudes and eigenfunctions during propagation toward deeper water. The second curve shows the results from propagating the source from water of 2.5-km depth (just beyond the shelf) out to the site in 3.4 km of water, maintaining a constant energy flux. The peaks at 0.7 and 0.9 Hz now match up, suggesting the higher-order peaks are associated with this second process of maintaining the energy flux as the position (in frequency) of the minimums of the group velocity curves for each mode shifts with the changing water depth. Our modeling efforts suggest that it is not possible to model the location in frequency of these higher-order peaks, without either changing the water depth in the model (to 4km depth) or else by allowing for propagation of modes down slope.

5.2 Interelement Microseismic Coherence

The coherence between pairs of instruments shows peaks and troughs that correspond to the peaks in the power spectrum (Figure 8). The coherence appears mainly controlled by the measurement signal-to-noise ratio. Coherences measured between the more closely separated instruments are similar, except some instruments are noisier than others. This measurement of the coherence contrasts greatly with measurements between closely spaced instruments on the Pacific seafloor. Instruments separated by 2 km on the Pacific seafloor are incoherent above 0.2 Hz (Webb et al, 1991). Schreiner and Dorman suggest scattering of energy from Rayleigh modes into Stoneley (sediment) waves controls the coherence observed across a very small (150-m aperture) seafloor array of seismometers. They observe a very different structure to the coherence than is seen in the Arctic measurements (Schreiner and Dorman, 1990).

In this record, the phase difference between the "white" instrument and either the "blue" or "green" instruments is very small (< 5) in the band from 0.1 to 0.7 Hz (the band for which the coherence is significantly different from zero for these pairs of instruments). The small phase differences observed suggest propagation nearly broadside to the array. We will assume a propagation velocity near 1.5 km/s consistent with oceanic Rayleigh modes above 0.2 Hz. Larger phase velocities are possible that would suggest larger angles between the direction of propagation and the orientation of the array. We infer the direction of propagation of these waves must be from either about 15° (true), suggesting we are seeing energy that has propagated across Alaska from the stormy Gulf of Alaska or from about 200° (true) and from the Norwegian Sea. The uncertainties in the timing of the instruments and the errors in the phase measurements preclude differentiating between the two azimuths.

Wave-number spectra generated from data from several large continental seismic arrays suggest microseism energy is primarily associated with surface wave modes (Cessaro and Chen, 1989). These studies also identified the Gulf of Alaska as a common source for microseisms. We cannot rule out energy associated with body waves; body waves from distant sources propagate at velocities greater than 7 km/s, and would generate little phase lag across the array. The coherence between the red and white instruments is above 0.95 in the spectral peaks below 0.4 Hz. At low frequency we would expect to see essentially perfect coherence between instruments, because the wavelengths of Rayleigh waves are so long (30 km at periods near 10 s).

The coherence in each of the spectral peaks allows us to put upper bounds on the beamwidth of these signals. Signals from varied directions add incoherently (in the absence of scattering effects), so the coherence is less between instruments in a wave field with a broader distribution of propagation directions. The constraint on the beamwidth is weak at low frequency, because the wavelengths of the signals are large compared to the distance between the instruments and the phase differences are small. We model the microseism wave field as a single mode with a phase speed of 1.5 km/s, a directional spectrum that is uniform within an angle 2ϕ, and zero outside this angle, and ask what the behavior of the coherence is as a function of frequency and the half beamwidth parameter (Figure 14). The figure shows the coherence corresponding to the frequencies 0.1, 0.25, 0.5, and 1.2 Hz. At 0.1 Hz, the observation that the coherence is above 0.9 does not constrain the directional spectrum at all. At 0.25 Hz, a coherence of 0.95 constrains the halfwidth angle to less than 30°, at 0.5 Hz, a coherence of 0.8 requires a halfwidth angle of less than 15°, and at 1.18 Hz, a coherence of 0.35 constrains the halfwidth to be less than about 12°. Since we believe the coherence is reduced by electronic noise, we infer from these calculations, that the energy in the microseism peak is propagating from a narrow range of directions at least at frequencies above 0.5 Hz. This is consistent with one large, distant source (in the Gulf of Alaska). The low energy throughout the spectrum is also consistent with distant sources, and indeed the coherences observed preclude significant local sources (which would tend to make the wave field more isotropic).

5.3 Very Low Frequency Waves

The energy in the pressure spectra from the Arctic seafloor increases rapidly at periods longer than about 50 s (Figures 6 through 8). Pressure spectra from sites on the floor of both the Atlantic and the Pacific show a similar rapid rise in spectral levels at long periods, but the spectra from the three oceans differ in subtle, but important ways. The Arctic spectrum is between 20 and 30 dB quieter than a typical spectrum from the Pacific at frequencies near 0.01 Hz and about 10 dB lower than typical spectra from an Atlantic site. However, the spectra are more similar in amplitude at frequencies below 0.001 Hz suggesting some mechanism to maintain a uniform spectral level at these very low frequencies (Figure 7).

Are the pressure signals we see at the seafloor related to measurable displacements of the surface of the ice? Gravity meter measurements of vertical displacement can be associated with propagating waves in the ice (LeSchack and Haubrich, 1964; Hunkins, 1962). The properties of waves in ice over water (flexural-gravity waves) are well understood. At short periods the rigidity of the ice determines the phase speed. At long periods, the waves are essentially identical to normal ocean waves (Hunkins, 1962; Davys et al, 1985). There is a local minimum in the group velocity for waves on typical Arctic ice (thickness 2.5 m) between a 20- and 35-s period and the on-ice gravity-meter measurements show a peak in the acceleration spectrum in the same band. The rms displacement in the band from 0.01 to 0.05 Hz is a few tenths of a millimeter. Hunkins was able to demonstrate phase propagation near a 35-s period at about 38 m/s (Hunkins, 1962).

The pressure signal from ocean waves or from coupled ocean-ice waves attenuates with depth with an e-folding scale equal to the inverse wave number. Pressure spectra measured at sites on the seafloor of both the Pacific or the Atlantic

are energetic at very long period, with a precipitous decrease above a corner frequency which depends only on the water depth above the site (Webb and Cox, 1986; Webb et al, 1991). This frequency corresponds to a wave number equal to the inverse water depth. The water depth over the instruments in the Arctic was about 3400 m, and the corner frequency about 0.0075 Hz. The Arctic pressure spectra do appear to exhibit a more rapid fall with increasing frequency above 0.008 Hz, although the spectrum is always very "red" in this low- frequency band. The presence of the ice introduces a negligible change in the corner frequency for this water depth. Below the corner frequency, we can infer the sea surface displacements corresponding to the Arctic seafloor pressure signals directly. One Pascal in pressure corresponds to 0.1 mm of surface displacement. LeSchack and Haubrich (1964) measured displacement spectral densities at 0.01 Hz between 3 and 10 mm^2/Hz. Our measurements of the pressure spectrum show values near 50 Pa^2/Hz at 0.01 Hz corresponding to displacement spectral densities after correcting for the decay from the surface of about 1 or 2 mm^2/Hz. The on-bottom pressure measurements in this band are consistent with displacement measurements made 30 years ago. The measurements of LeSchack and Haubrich do not extend further in frequency so we are unable to compare the surface and bottom measurements at a longer period.

There have been several recent measurements of tilting and straining of the ice in the Arctic. The spectra of both tilt and horizontal strain exhibit a broad peak near 35-s period (Czipott and Podney, 1989; Williams et al, 1989). A persistent, small bump, or ledge in the Arctic pressure spectrum near 50 to 60 s in period, may be the seafloor manifestation of this peak, obscured by the hydrodynamic filtering. We can use the flexural-gravity wave dispersion relation to predict the pressure signal from the strain and tilt measurements. Figure 15 shows the relationship between the tilt spectrum in the direction of propagation and the pressure spectrum. The figure shows two curves, one relating the tilt to pressure fluctuations near the sea surface and the second to pressure fluctuations at the seafloor. The pressure signal at the seafloor at periods shorter than 50 s is much reduced because of the hydrodynamic "filtering" above the corner frequency. Estimates of the seafloor pressure spectrum at four frequencies associated with the tilt spectrum measured by Czipott and Podney on the ice near Greenland are plotted in Figure 7. The tilt measurements predict very similar amplitudes for the flexural-gravity waves as do the pressure measurements. The authors report the tilt measurements have a large uncertainty in calibration.

The strain measurements appear much noisier than the tilt measurements in the flexural-gravity wave band. The relationship between horizontal strain and the amplitude of the flexural gravity waves is complicated because it depends on the elastic parameters in the ice, and the thickness of the ice (Czipott and Podney, 1989). The strain measurements predict larger flexural-gravity wave amplitudes at long periods than the tilt measurements. It appears that the strain spectrum may depend on other physical processes such as deformation by the wind and internal waves.

Our understanding of these waves requires an explanation for the very similar amplitudes seen in the Norwegian Greenland Sea and the Beaufort Sea and the small variability in amplitude from day to day. We see only a factor of 2 variability in energy in the long wave band (Figure 16). There are three possibilities: (1) the loss during propagation is so slight that the two areas see the same wave field, (2) there is a universal source such as the force of wind on the ice, that generates and maintains a uniform level, and (3) inadequate data has failed to identify the true variability in the wave field.

Hunkins related the waves he detected to forcing by the local wind. Haubrich and LeSchack reexamined this problem and found little variation in the spectrum of ice displacement between windy and calm days (LeSchack and Haubrich, 1964). They concluded that forcing by local winds was of secondary importance and that the long period energy they saw had propagated in from the open ocean. Squire (1986) measured the oscillations of the ice on a lake under the influence of the wind. We see no correlation between the local surface winds measured at the ice camp and the pressure record below 0.01 Hz (Figure 16). The amplitude varies about a factor of 2 over the 2-week period. Czipott and Podney (1989) also found no correlation between the local wind and ice tilts, and suggested the ice is usually too thick to respond to local wind forcing with other than essentially static deformation. Propagation directions inferred from the tilt measurements suggested propagation through the ice from the open sea. This issue is discussed further in section 6.3.

6. BASIC Seismic Measurements

The onshore seismograms exhibited stationary microseismic noise spectra upon which was superimposed energy from a variety of regional and distant teleseisms. The onshore station was a raised gravel drill pad built atop permafrost, and located directly on the shore of the frozen Beaufort sea (Figure 17). The pad served as an oil pumping and production facility. The 3 component 1 Hz seismometers were frozen onto a 1/2" thick steel plate which, in turn, was hard frozen onto the ice that thickly covered the ground surface. This arrangement was also used for the on-ice mea-

surements, and in all cases, the seismometers were surrounded on top and sides by boxes, and the entire sensor arrangement then covered with snow. A large snow berm was built around this, using heavy equipment provided courtesy of Arco, for the purpose of eliminating wind noise to the largest possible extent.

6.1 Teleseisms

The catalog of teleseisms detected at Arctic latitudes is relatively sparse. It had been a subsidiary goal of this project to record any such events, both to buttress global seismic tomographic efforts, as well as to enable studies of propagation of seismic energy beneath the Brooks Range and N. Slope of Alaska. We further hoped that the quiet subice environment would make it possible to detect teleseisms on the seafloor of lower magnitude than is typically possible.

A global map of focal mechanisms for March 1990 appears in Figure 18. The best-recorded of the distant teleseismic events, both ashore, and in the seafloor DPG records, are detailed in Table 1. Figures 19 and 20 contain the focal mechanism solutions for the Costa Rica, Hokkaido, and Kermadec events. Figure 21 shows the locations of Alaskan regional earthquakes for March 1990. In addition to background seismicity, several volcanic events were due to the continued eruption of Mt. Redoubt volcano near Anchorage. The best recorded (by the BASIC Deadhorse station) of the regional events are listed in Table 2.

Table 1: Distant Teleseisms Recorded

Location	Latitude	Longitude	Depth	M_{SZ}/M_B	Date	Origin Time	Where Recorded
Gulf of California	24.897 N	109.035 W	10 km	6.1/5.5	16 March 1990	15:52:49.0	Deadhorse
Bonin Islands	27.220 N	141.605 E	47 km	5.0/5.8	20 March 1990	01:12:28.3	Deadhorse, APLIS
Kermadec Islands	31.092 S	179.093 W	145 km	?/6.2	21 March 1990	16:46:05.4	Deadhorse, Seafloor
Venezuela Coast	10.825 N	65.389 W	24 km	4.6/5.4	21 March 1990	18:51:09.5	Deadhorse, Seafloor
Costa Rica	9.919 N	84.828 W	22 km	7.0/6.2	25 March 1990	13:23:7.8	Deadhorse, Seafloor
Tajikistan	37.034 N	72.942 E	33 km	6.3/6.0	25 March 1990	14:17:18.8	Deadhorse, Seafloor
Costa Rica	9.591 N	84.659 W	41 km	5.4/5.6	25 March 1990	21:35:30.5	Deadhorse, Seafloor
Kurile Islands	45.331 N	150.204 E	50 km	4.1/5.2	29 March 1990	04:34:04.2	Deadhorse
Mariana Islands	16.572 N	145.831 E	24 km	4.6/5.3	29 March 1990	14:15:44.8	Deadhorse
Mariana Islands	16.546 N	145.867 E	33 km	?/4.8	29 March 1990	14:36:29.2	Deadhorse
Tajik/Xinjiang	39.408 N	73.256 E	25 km	5.1/5.4	29 March 1990	16:19:15.8	Deadhorse
Hokkaido Coast	42.891 N	146.969 E	21 km	5.8/5.9	31 March 1990	19:31:42.7	Deadhorse

A three component seismogram (after instrument response correction) from Deadhorse, for the first of the 25 March 1990 Costa Rica earthquakes, is found in Figure 22. In addition to such high quality conventional short period seismograms as recorded ashore at Deadhorse, it was (surprisingly) possible to clearly pick P and S arrivals for the Bonin Islands earthquake of 20 March 1990 from the on-ice seismograms recorded at APLIS/90 (Figure 23). The observation of and S wave phase on the ice suggests there is some rigid coupling between the sea ice and coastline.

Excellent DPG seismic records were recorded on the seafloor from a number of distant teleseisms, and the detection threshold permitted the anomalous spectral levels associated with the magnitude 4.6/5.4 Venezuela earthquake of 21 March 1990 to be detected. To our knowledge, this is one of the smallest teleseisms detected on the seafloor. A seafloor DPG seismogram from the period of the first Costa Rica event of 25 March 1990 appears in Figure 24. P and S arrivals have been picked from standard travel time curves, and possible PPP and SKP phases have been identified as well. The coda for this seafloor-detected event lasted more than two hours.

Although the distance of 85° from the source is of relatively small interest to global tomographers, the detection of such teleseisms bodes well, in future, for using the Arctic seafloor for deep earth geotomography studies.

6.2 Microseisms

Examination of the ambient noise spectrum for the onshore station reveals a typical continental structure, with spectral levels similar to other quiet continental sites. Within the frequency band of just below 10^{-2} to about 5×10^{0} Hz, the dominant stationary ambient signal is that due to double frequency microseisms. A time spectral history is seen in Figure 25. Here, superimposed on the stationary signal are greatly elevated transient spectral levels due to the Costa Rica and Tajikistan teleseisms.

Table 2: Regional Events Recorded

Location	Latitude	Longitude	Depth	M_{SZ}/M_B	Date	Origin Time	Where Recorded
Mt. Redoubt	60.534 N	152.870 W	143 km	M_L=3.4	16 March 1990	05:04:47.9	Deadhorse
Mt. Redoubt	60.534 N	152.870 W	?	M_L=1.8	18 March 1990	15:04:51.1	Deadhorse
Mt. Redoubt	60.534 N	152.870 W	?	M_L=1.8	20 March 1990	15:11:20.?	Deadhorse
Kenai Peninsula	59.371 N	148.122 W	12	?/2.8	21 March 1990	09:39:35.8	Deadhorse
Mt. Redoubt	60.534 N	152.870 W	?	?	21 March 1990	11:25:??.?	Deadhorse
Central Alaska	63.379 N	151.396 W	11 km	?/3.2	21 March 1990	15:51:46.9	Deadhorse
Mt. Redoubt	60.534 N	152.870 W	?	?	29 March 1990	01:33:??.?	Deadhorse
South of Alaska	53.768 N	159.700 W	33 km	?/4.5	29 March 1990	09:14:33.7	Deadhorse
Southern Alaska	59.987 N	153.278 W	155 km	?/3.5	29 March 1990	12:20:55.0	Deadhorse

Double frequency microseismic power spectral densities are persistently about 1.5×10^{-10} cm^2 s^{-2} Hz^{-1} for both vertical and N-S horizontal components, with the peak level typically centered near 5 s period. The E-W horizontal component generally has about half the power of the vertical and N-S, i.e. there is overall polarization of the incident wavetrains. A typical stationary part of the spectrum for the vertical component at Deadhorse is found in Figure 25. Compared against a noisy hard rock continental location, the double frequency peak at Deadhorse, in the vertical component, is down by about 30 dB, but is well within expected values for a quiet hard rock continental location (Aki and Richards, 1980). The other major features of the ambient stationary power spectrum are a bench in power near 2.18 s (0.46 Hz) (down about 12 dB from the double frequency peak), then an abrupt fall at 1 s (1 Hz) to a plateau down about 20 dB from the peak, which continues to about 0.6 s period (1.67 Hz). At frequencies higher than this, there is an abrupt increase in noise.

The propagation of microseismic energy into the continent is inadequately modelled by the pseudoacoustic eigenanalysis previously used to describe the structure of the microseismic spectrum on the seafloor. There is no direct correspondence between the seafloor higher order microseismic peaks, and the onshore spectral features. Indeed, onshore, there are no clear higher order peaks at all. No adequate model for this behavior has yet been constructed, and this part of the work will continue.

Another striking feature of the onshore stationary spectrum is a clearly delineated, nearly perfect delta-function-like spectral line at a period of 12.01 s (0.083 Hz). This is located at the high frequency extreme of the noise notch, and is of appropriate period to be considered a candidate for excitation due to single frequency microseisms. Some points must be made. First, this small peak, rising about 0.4 dB above ambient levels, cannot be seen at all in the non-robust spectral estimates, and is only found in these robust spectra. The overall noise level in the notch, for the conventional non-robust spectra is up about 0.8 dB from that seen in the robust estimates. This is due to a combination of either outliers in the time series, or effects of short sections of non-stationary data drawn from a different statistical population than the stationary ambient noise process (this explanation is most likely). Second, it seems highly unlikely that single frequency microseisms would appear with such a perfect monochromatic character. Previously, single frequency microseisms have always been seen as broad spectra peaks. While Figure 23 may contain the highest resolution spectral estimate yet obtained in this band, the physics of microseismic generation would still suggest a broadening of this peak due to the integrated effects of wave trains of different period hitting distant coasts and then coupling into the rock waveguide as Rayleigh waves.

One alternative explanation for the monochromatic peak is that it might be due to man-made causes. In particular, the Arco site at Deadhorse, Alaska, was an active production pad. It is possible that a pump, with very long period action, may be part of the oil extraction equipment. This remains conjecture, but we prefer to attribute this peak, not to single frequency microseisms, but to external causes. Having said this, it is curious, to say the least, that single frequency microseisms were detected, although at very small levels, on the seafloor pressure records, but not onshore, especially when the single frequency seafloor peak was down only about 15 dB from the double frequency peak.

6.3 Comparison Between Onshore and On-Ice Spectral Levels

Power spectral density levels for an ambient noise record on-ice at APLIS/90, and onshore at Deadhorse, Alaska, are plotted on a common scale in Figure 26. Both sets of spectra are for the vertical 1 Hz channels, and represent a one-

day-long time series section, for a period free of regional earthquakes and distant teleseisms. The difference between the traces is striking. The on-ice measurement noise floor in the microseismic band is too high to detect either single or double frequency microseisms. The major (and quite remarkable) feature of this spectrum is the intensely energetic and broad peak centered at about 30 s period (0.03 Hz). This is particularly surprising since the sensitivity of 1 Hz sensors rolls off dramatically at these periods, which serves to make it apparent how energetic this peak is. Scaled into more familiar terms, the spectral density exceeds 3 x 10^{-8} cm^2 s^{-2} Hz^{-1}.

The broad long period peak corresponds nicely with the seafloor pressure measurements, and the proposed flexural wave mechanism discussed previously. In particular, we refer to the hydrodynamic filtering of a sea surface disturbance at this period being responsible for the persistent bump in the seafloor pressure spectra. Ice tilt at periods near 35 s was detected by Czipott and Podney (1989), and by Williams et al (1989). It is evident that the on-ice geophones have detected ice flexure due to this same mechanism.

Webb et al (1991) have shown a relationship between pressure fluctuations on the seafloor of the western Atlantic and the average short period wave height along the shore of the central Atlantic. The model suggests a conversion from short to long-period energy in the surf zone by nonlinear mechanisms. The long-period energy then propagates to deep water as free waves. The ice is no barrier to these very long-period waves, however it is difficult to reconcile the similar amplitudes detected in the Beaufort and Greenland Seas, given the constricted geometry of the Arctic ocean straits. These long waves are only gently steered by bathymetry. The Norwegian Sea and the Beaufort Sea are not connected by a great circle path, the approximate propagation path for a long wave. Energy that has reached the Beaufort from the Atlantic must have either reflected from a shore line, or scattered from topography. Reflection of long-surface gravity waves from coastlines is usually not very efficient (Webb et al, 1991). We are considering whether another process that might generate long-period waves may be the action of atmospheric pressure fluctuations in shallow water. Wind can generate large-scale oscillating pressure fluctuations that propagate with the wind velocity. The phase velocity of long-period waves can be comparable to wind velocities in shallow water.

7. BASIC Conclusions

We have measured the amplitude of the pressure spectrum at the floor of the Beaufort sea in the frequency band from 0.0001 to 8 Hz. We found very quiet levels across the entire band. Both single-and double-frequency microseism peaks are obvious throughout the experiment. The microseism spectrum is remarkably stationary over 2 weeks. The double-frequency peak is subdivided into a least five peaks apparently associated with the propagation of individual seismoacoustic modes. The energy in the microseism peak is very coherent across the band. The phase relationship between instruments suggests a direction of propagation of about 15° (true) from a wide source region in the Gulf of Alaska, although incident energy from the Norwegian coast also cannot be ruled out. Large earthquakes generate wave trains that occasionally dominate the pressure spectrum at all frequencies. The earthquake spectra are peaked at about 25-s period.

At periods longer than 50 s, the spectrum rises abruptly because of pressure fluctuations caused by freely propagating gravity waves. The pressure measurements suggest wave heights similar in amplitude to that predicted from ice surface gravimeter and tilt measurements. The speculation in the literature suggest this long period energy propagates in from the open sea. Another possibility is wind forcing, possibly occurring primarily in shallow water. More work will be required before the source of long-period flexural-gravity waves in the Arctic is unambiguously identified.

Onshore measurements show the North Slope of Alaska has microseismic spectral density levels typical for those of quiet continental hard rock sites. There are no clear higher order double frequency microseismic modes detected onshore. The single frequency peak detected in the Beaufort seafloor is absent onshore, and replaced by an almost perfectly monochromatic line, which we prefer to attribute to man-made sources. A substantial number of both distant teleseisms, and regional earthquakes and volcanic events were detected onshore.

On-ice geophone measurements tend to confirm that flexural ice motion with a center period of about 30 s is likely to be responsible for the long period bench in the seafloor pressure spectrum. We have also demonstrated that it is possible to detect teleseisms on the surface of the ice, with the N-S component near the ice camp having clearly recorded both P and S phases from the Bonin Islands earthquake. The detection of the latter suggests there is a degree of rigid coupling between the sea ice and the shoreline.

Finally, we have also clearly demonstrated it is possible to detect teleseisms with a smaller noise threshold beneath the Beaufort Sea than beneath open oceans. A magnitude 4.6/5.4 event from off the coast of Venezuela was detected.

while very high quality seismic waveforms were returned from the magnitude 7.0/6.2 Costa Rica earthquake.

This project has immediately preceded the NOBS experiment, and the analysis of these data, as well as these initial findings, will play a significant role in clarifying the interpretation of the more complicated NOBS dataset. In particular, the single most important finding of BASIC, that in the absence of coupling of local wind stress to the water column, the power in the microseismic band falls precipitously, will have direct bearing on the NOBS experiment. Preliminary results from NOBS (B.T.R. Lewis, personal communication, 1993) indicate that there is no significant phase lag between local ocean surface gravity (wind) waves and microseismic waves detected on the bottom (the former having been measured by wave height sensors aboard the FLIP manned buoy). This is consistent with the BASIC results. We suggest that the greatest part of microseismic energy detected on the bottom may be due to very local sources. A small portion of the energy is converted into Rayleigh waves and propagates great distances. This part is represented by the diminished spectral density levels recorded beneath the Beaufort Sea. BASIC suggests that the greatest part of the bottom pressure disturbance due to surface nonlinear wave-wave interaction, however, is seen only locally directly beneath the storm center.

8. Refereed Publications and Papers Communicated

Webb, S.C., and A. Schultz. Very Low Frequency Ambient Noise at the Seafloor Under the Beaufort Sea Icecap, *J. Acous. Soc. Am.*, 91, No. 3, 1429-1439, 1992.

Schultz, A., S. Webb, B. Lewis. Spectral levels within the microseismic band beneath an ice covered sea. AGU Fall meeting, 1990.

Schultz, A., S. Webb. and B. Lewis. ULF spectra, non-stationarity and coherence in an ice-covered ocean. Conference on Natural Physical Sources of Underwater Sound, University of Cambridge, UK, 1990.

Dorman, L.M., J.A. Hildebrand, A. Sauter, A. Schreiner, B.T.R. Lewis, A. Schultz, and M. Dougherty. The NOBS experiment (Noise on Basalt and Sediment). AGU Fall meeting, 1991.

9. Budget Details

The major budget categories include salaries for the P.I.(s), graduate student (the major part of the latter was used to pay Dr. Luciana Astiz, a post-doctoral researcher working on the seismometer data with the approval of the contract officer), and project engineer; the expenses related to operating ice camp APLIS/90 (inclusive of ice camp operations fees, helicopter usage, support staff at APLIS/90 used directly by this project; snowmobile and communications equipment; transport from Deadhorse to the ice camp; staging operations at Deadhorse); a subcontract to the University of California San Diego, Scripps Institution of Oceanography (Dr. Spahr Webb) to provide Dr. Webb's services and the configuration and use of four free-fall autonomous recording differential pressure gauges (DPGs); capital equipment and modifications, including purchase of the bearing option electronics and transducer for our EG&G acoustic release deck unit as well as appropriate Arctic housing for the PASSCAL seismometers and REFTEK dataloggers obtained from the PASSCAL Instrumentation Center at Lamont; travel to permit Drs. Schultz and Webb to transit to Prudhoe Bay, and then transfer to APLIS/90 (two return trips, one for instrument deployment and a second for instrument recovery - which was far cheaper than staying at the ice camp for the 2 week+ duration of the experiment); and communication, shipping and postage. The equipment (PASSCAL instruments, Arctic gear, SIO equipment) was shipped from Seattle to Valdez, Alaska by barge, then forwarded by truck up the haul road to the North Slope (except for the most sensitive electronics, which were air shipped).

10. Literature Cited

S. C. Webb and C. S. Cox, "Observations and modeling of seafloor microseisms," J. Geophys. Res. 91, 7343-7358, 1986.

G. H. Sutton and N. Barstow, "Ocean bottom ultralow frequency (ULF) seismo- acoustic ambient noise, 0.002 to 0.4 Hz," J. Acoust. Soc. Am. 87, 2005-2012, 1990.

K. A. Hasselmann, "A statistical analysis of the generation of microseisims," Rev. Geophys. Space Phys. 1, 177-210. 1963.

B. M. Buck and J. H. Wilson, "Near field noise measurements from an Arctic Pressure ridge," J. Acoust. Soc. Am. 80, 256-264, 1986.

A. R. Milne, J. H. Ganton, and D. J. McMillan, "Ambient noise under sea ice and further measurements of wind and temperature dependence," J. Acoust. Soc. Am. 41, 525-52, 1967.

C. Makris and 1. Dyer, "Environmental correlates of pack ice noise," J. Acoust. Soc. Am. 80, 1434 1440, 1986.

K. Lewis and W. W. Denner, "Arctic ambient noise in the Beaufort Sea: seasonal space and time scales," J. Acoust. Soc. Am. 82, 988-991, 1987.

K. Lewis and W. W. Denner, "Arctic ambient noise in the Beaufort Sea: seasonal relationships to sea ice kinematics," J. Acoust. Soc. Am. 83, 549-565, 1988.

D. Prentiss and J. I. Ewing, "The seismic motion of the deep ocean floor," Bull. Seism. Soc. Am. 53(4), 765-781, 1963.

S. C. Webb, X. Zhang, and W. Crawford, "Infragravity waves in the deep ocean," J. Geophys. Res. 96(2), 2723-2736, 1991.

A. LeSchack and R. A. Haubrich, "Observations of waves on an ice covered ocean," J. Geophys. Res. 69(18), 3815-3821, 1964.

P. Crary, R. D. Lotell, and J. Oliver, "Geophysical studies in the Beaufort Sea, 1951", Trans. Am. Geophys. U. 33(2), 211-216 (1952). Hunkins, "Waves on the Arctic Ocean," J. Geophys. Res. 67(6), 2477-2489, 1962.

V. Czipott and W. N. Podney, "Measurements of fluctuations in tilt of Arctic ice at the CEAREX Oceanography camp: experimental review, data catalog and preliminary results," Final Tech. Rep. PD-LJ-89-369R, p. 53, Physical Dynamics, Inc., La Jolla, CA, 1989.

R. S. Williams, S. Moore, P. Wadhams, and M. Beard, Measurements of Strain in Sea Ice during FRAM 3 (Scott Polar Research Institute, Cambridge, 1989, Vol. 89-1.

C. S. Cox, T. K. Deaton, and S . C. Webb, "A deep sea differential pressure gauge," J. Atm. Oceanic Tech. 1(3), 237-246, 1984.

S. C. Webb, "Long period acoustic and seismic noise and ocean floor currents," IEEE J. Oceanic Eng. 13, 263-270, 1988.

S.C. Webb, "Very low frequency sound studied using multielement seafloor arrays," in Proceedings of Natural Physical Sources of Underwater Sound, edited by B. Kerman (Cambndge U.P., Cambridge, 1990) (in press).

Kutschale, "Arctic hydroacoustics," Arctic 22, 247-264, 1969.

C. Kibblewhite and K. C. Ewans, "Wave wave interactions microseisims and infrasonic ambient noise in the ocean," J. Acoust. Soc. Am. 78, 981-994, 1985.

E. Keenan and 1. Dyer, "Noise from Arctic ocean earthquakes," J. Acoust. Soc Am. 75, 819-825, 1984.

B. Baggereor and R. Falconer, "Array refraction profiles and crustal models of the Canada Basin," J. Geophys. Res. 87(B7), 5461-5476, 1982.

L. N. Kennett, "Guided wave attenuation in laterally varying media," Geophys. J. Int. 100, 415 422, 1990.

F. Panza, "Synthetic seismograms: the Rayleigh waves model summation,"J.Geophys.58, 125-145, 1985.

E. Schreiner and L. M. Dorman, "Coherence length of seafloor noise: effect of ocean bottom structure," J. Acoust. Soc. Am. 88, 1503-1514, 1990.

Schmidt and W. A. Kuperman, "Estimation of surface noise source level from low frequency seismoacoustic ambient noise measurements," J. Acoust. Soc. Am. 84, 2153-2162, 1988.

Chiaruttini, G. Costa, and G. F. Panza, "Wave propagation in multilayered media: the effect of waveguides in oceanic and continental earth models," J. Geophys. Res. 58, 189-196, 1985.

A. Drake and B. A. Bolt, "Finite element modeling of surface wave transmission across regions of subduction," Geophys. J. Int. 98, 271-279, 1989.

L. N. Kennett, "Guided wave attenuation in laterally varying media," Geophys. J. Int. 100, 415 422, 1990.

A. Kuperman, M. B. Porter, and J. S. Perkins, "Rapid computation of acoustic fields in three-dimensional ocean environments," J. Acoust. Soc. Am. 89, 125-144, 1991.

T. Lacoss, E. J. Kelly, and M. N. Toksoz, "Estimation of Seismic Noise Structure Using Arrays," Geophysics 34 (1), 21-38, 1969.

Aki and P. G. Richards, in Quantitahue Seismology Theory and Methods (Freeman, San Francisco, 1980) , p. 303.

K. Cessaro and W. W. Chen, "Wide-angle triangulation array study of simultaneous primary microseism sources" J.Geophys.Res., Bll, 15555-15563, 1989.

W. Davys, R. J. Hosking, and A. D. Sneyd, "Waves due to a steadily moving source on a floating ice plate," J. Fluid Mech. 158, 269-287, 1985.

A. Squire, "Wind over ice: a mechanism for the generation of ice-coupled waves," in Ice Technology, Proceeding of the Ist International Conference (Springer-Verlag, Berlin, 1986), pp. 115-127.

11. Figure Captions

Figure 1. Location map in polar projection, showing approximate position of ice camp APLIS/90, and the continental seismic station established near Deadhorse, Alaska.

Figure 2. The position of ice camp APLIS/90 as the ice drifted during days 072 through 095, 1990. The large symbols represent the drop locations of the free-fall autonomous ocean bottom differential pressure gauges. Different small symbols are plotted on the trackline to separately identify each calendar day.

Figure 3. The trackline of the drift of ice camp APLIS/90 (small symbols) on the day of deployment (day 076, 1990), and the locations of the four seafloor instruments, "red", "green", "blue", and "white". The area shown is a 1 square nautical mile region. APLIS/90 positions were fixed by reference to GPS coordinates, while the seafloor positions were tied into the geodetic frame by use of a large baseline acoustic navigation system installed at the ice camp. The relative positions of the instruments are known to a few meters.

Figure 4. A free-fall autonomous ocean bottom differential pressure gauge instrument as configured during seafloor deployment. The glass flotation spheres float 30 m above the instrument to provide clearance between the acoustic transponder/release (connected to the drop weight), and keels in the ice cap at the surface.

Figure 5. Typical seafloor pressure timeseries. This is an 8 minute long section showing ambient noise as recorded at instrument "green".

Figure 6. Pressure power spectral density of seafloor ambient noise as recorded on instrument "white", plotted on a linear frequency scale. This was generated by taking the ensemble average of time series sections of length 160,000 points, with 70% overlap between sections, and using a total of 691,200 data points. A time-bandwidth product 4 prolate spheroidal taper sequence was used to shape the endpoints of the time series sections. Following ensemble averaging, each six adjacent frequencies were band-averaged. The estimate shown is of the statistically robust type, using a modified form of Huber weighting. Significant spectral peaks are seen centered at 13 s, 6.6 s, 3.3 s, 1.9 s, and higher order terms. This method of spectral analysis is used throughout this work.

Figure 7. Pressure spectrum from an Arctic ocean bottom pressure gauge, showing multiple microseismic peaks and rising energy toward low frequencies due to flexural-gravity waves (infragravity waves). The confidence limits refer to a range of estimates of the pressure spectrum inferred from tilt measurements from ice in the Norwegian Sea (Czipott & Podney, 1989). Pressure spectra from sites in the Atlantic and Pacific oceans are also shown.

Figure 8. Pressure spectra (top panel), coherence (middle), and phase (bottom) between instruments "red" (dashed) and "white" (solid) during one 4-h record. Spectral peaks correspond to bands of high coherence between instruments. The small phase lags detected within the peaks are consistent with wave propagation broadside to the nearly linear array.

Figure 9. Contour and surface plots showing the evolution of the pressure spectrum measured with instrument "green" during the experiment. The stability of the shape and amplitude of the microseism peak is evident. The wave trains from several large earthquakes generate transitory broad peaks centered around 25 s period.

Figure 10. Spectral density in three bands near 0.15 Hz vs. time in hours from the start of the experiment. The energy in this peak in the microseism band varies by 10 dB over the 2 week period. The peak at 192 h is caused by the wave trains from a pair of large earthquakes.

Figure 11. (left) Phase velocity for the 20 Rayleigh modes in a realistic model for the ocean and seafloor at the Arctic site. Also shown (dashed) phase velocity for modes in a model ocean with a rigid seafloor. (right) model used in the calculations based roughly on Baggereor and Falconer (1982), compressional velocity (solid), shear velocity (short dash), and density (long dash). The seafloor is at 3-4 km depth.

Figure 12. Vertical (solid) and horizontal (dash) eigenfunctions for the first 4 modes at 0.125 Hz. The eigenfunction for the 3rd mode resembles the fundamental mode eigenfunction in a model ocean with a rigid seafloor since there is a cosine dependence with depth for the vertical velocity with a zero crossing near the seafloor, and a sine dependence

for the horizontal component with a maximum at the seafloor. The fundamental mode in this model is a Stoneley wave with an exponential decay of the eigenfunction away from the seafloor. The 4th mode is essentially a pure Rayleigh wave within the rock.

Figure 13. Typical Arctic seafloor pressure spectrum (solid line). Results from modelling the excitation of modes at the shelf break in an ocean of constant depth (dash-dot line) and in an ocean where the depth varies from a depth of 2.5 km at the source to 3.4 km at the observation site (dashed).

Figure 14. Coherence vs beam width and frequency between instruments 1.5 km apart. Model assumes a uniform directional distribution within an angle 2ϕ, and no energy outside the angle. Coherence shown for 4 frequencies (0.1, 0.25, 0.5, and 1.1 Hz). Coherence is nearly independent of beamwidth at low frequency.

Figure 15. Conversion from a tilt spectrum to pressure spectrum at the sea surface (solid) and seafloor (dashed). Units are dB relative to 1 Pa/arcsecond.

Figure 16. Root-mean-square pressure signal between 0.001 and 0.03 Hz vs time in 4-h segments. Also shown (dashed) the wind velocity measured at the APLIS ice camp over the same interval.

Figure 17. Location of onshore seismometer vault at Arco production facility, Deadhorse, Alaska. A remote site on the coastline of the (frozen) Beaufort Sea, the drill pad was generally unvisited by personnel, and access was under tight security, making it possible to obtain high quality ambient noise records.

Figure 18. Focal mechanisms for March 1990. Teleseisms from Costa Rica, Gulf of California. Bonin Islands, Tajikistan, and Kermadec were all detected by the station set up at Deadhorse, Alaska. The Bonin Island event was also recorded by the 1 Hz seismometers set up on the ice near APLIS/90. Substantial local (Alaskan) seismicity was detected at Deadhorse, as were events associated with the volcanic eruptions of Mt. Redoubt near Anchorage.

Figure 19. Focal mechanism solution and waveforms for Costa Rica (top) event of 25 March 1990, and Hokkaido event (bottom) of 31 March 1990.

Figure 20. Focal mechanism solution and waveforms for Kermadec event (top) of 21 March 1990, and Costa Rica event (bottom) of 25 March 1990.

Figure 21. Location of Alaskan regional earthquakes. A number of these were detected by the BASIC station at Deadhorse (Table 2).

Figure 22. Three component seismograms from Deadhorse, Alaska corresponding to arrival of Costa Rica teleseism. Correction for instrument response has been made.

Figure 23. Three component seismograms from ice camp APLIS/90, corresponding to arrival of Bonin Island teleseism. P and S wave arrivals are evident in the N-S horizontal channel. This is not detected on the E-W horizontal, and appears only as an increase in high frequency energy in the vertical channel.

Figure 24. Ocean bottom pressure record from instrument "Green" during the arrival of the teleseismic wave train from the Costa Rica earthquake. P, S, and possible PPPP and SKP phases are evident, with the coda persisting for more than two hours.

Figure 25. Spectral density history for vertical 1 Hz seismometer at Deadhorse, Alaska, for 24 hour period spanning 1990 Day 084. Each spectrum is for a time period of 7.5 minutes. The persistent double frequency microseismic peak is evident, atop which are elevated spectral density levels corresponding to the arrivals of teleseisms from Costa Rica (M_s=7.0, Δ=72°) and Tajikistan (M_s=6.3, Δ=68°).

Figure 26. Statistically robust (Huber weighting) power spectral density estimate (±1 standard error, calculated using non-parametric Jackknife technique), for a total of 10 days of vertical component seismogram (6,912,000 data points). This is an ensemble of 826 16,384-point-long time series sections. A high resolution time-bandwidth product 1 prolate

spheroidal taper sequence was used to shape the time series, and 50% overlap between time series sections was used to create the ensemble average. Each 4 adjacent frequencies were band-averaged. Each spectral estimate represents 6,608 degrees-of-freedom, making it possible to resolve extremely fine details in this spectral density plot.

Figure 27. Spectral density levels for 1 Hz vertical seismometer at Deadhorse, Alaska (bottom curve), and for identical instrument set up on ice near ice camp APLIS/90 (top curve). The dominant signal for the shore-side station is the double frequency microseismic peak. This station is relatively quiet for a continental location. The small delta-function like spectral line near 13 seconds is statistically significant. Although it falls exactly in the band expected for the single frequency microseismic peak, the nearly perfect harmonic character leads us to interpret this line as due to pumping machinery near the oil production well pad where the instrument was positioned. The dominant signal for the ice station is a strong peak near 30 seconds, which we interpret as flexure of the ice due to infragravity waves. The noise floor in the microseismic band is just above the shore-side microseismic level, and no microseisms are detected on the surface of the ice.

End Main Body Of Final Report

Figures to Follow

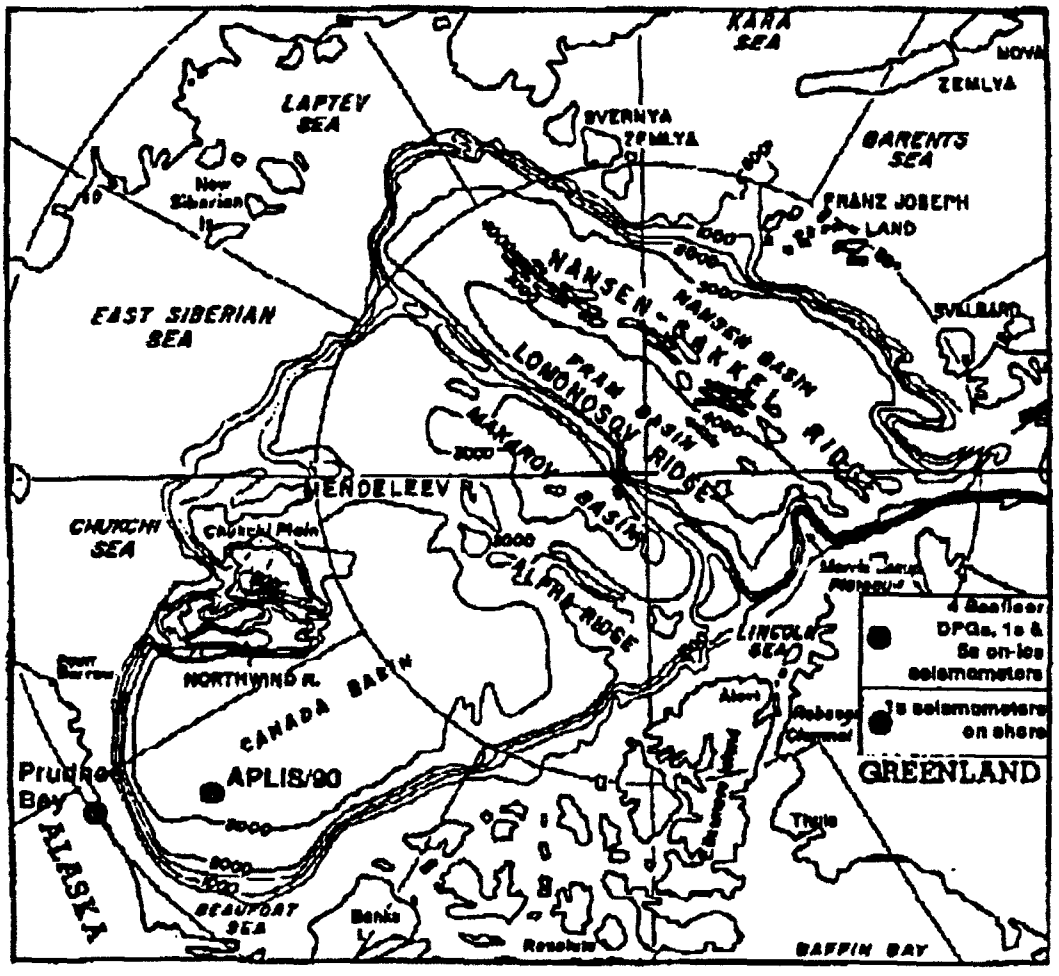

BASIC/90 Array Locations

Figure 1

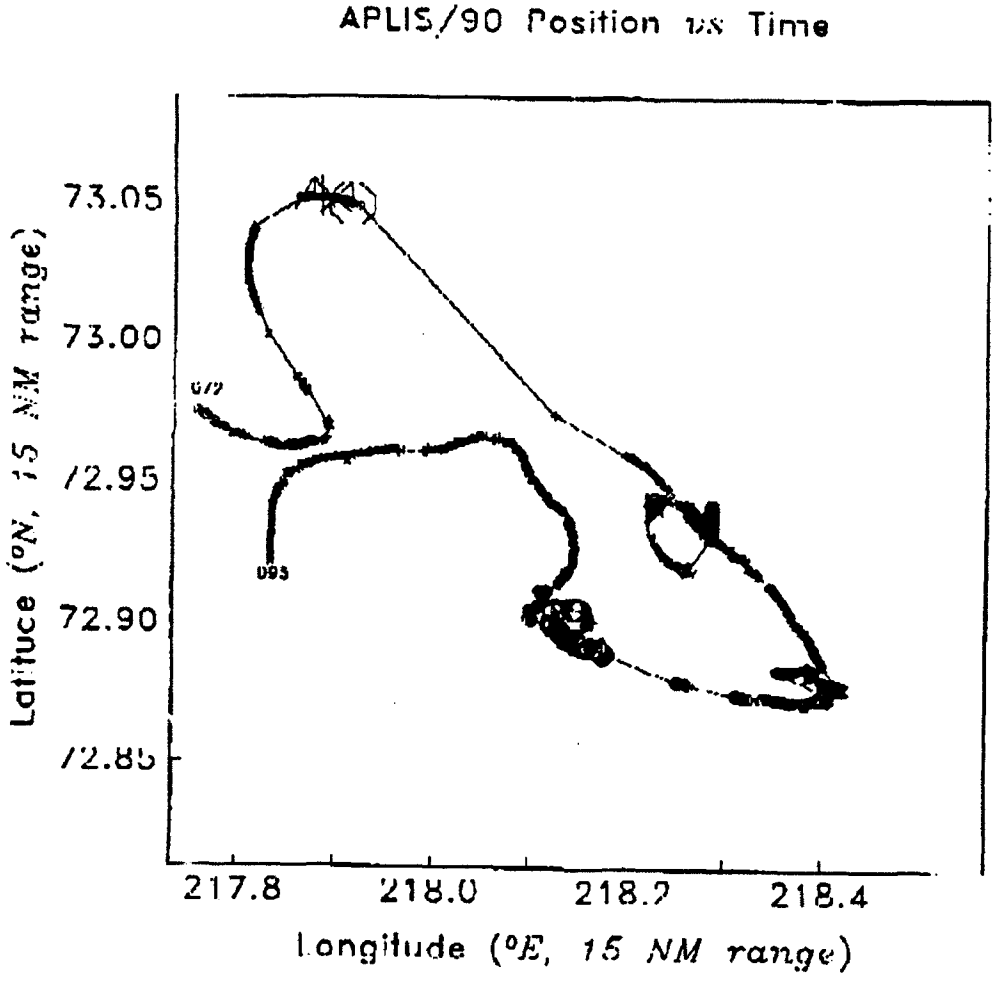
APLIS/90 Position vs Time
73.05
73.00
72.95
72.90
72.85
Latitude (°N, 15 NM range)
217.8
218.0
218.2
218.4
Longitude (°E, 15 NM range)

Figure 2

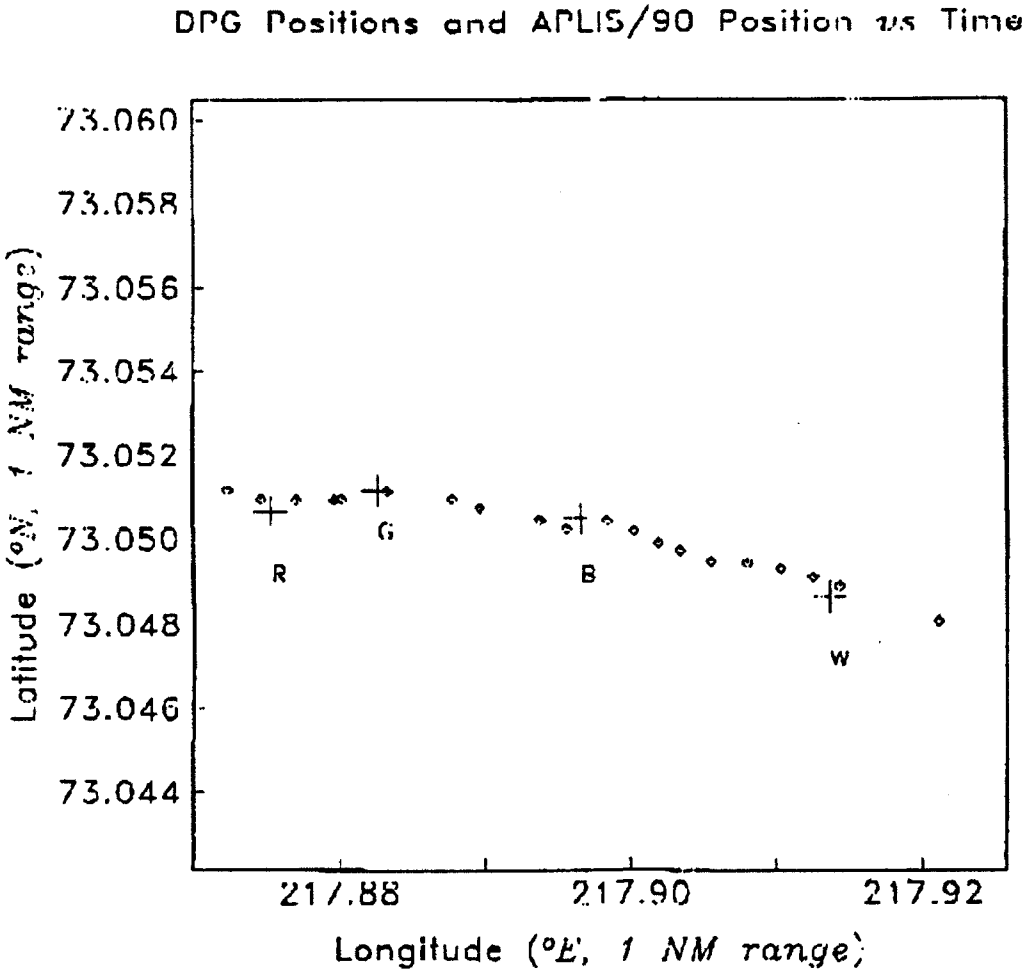
DPG Positions and APLIS/90 Position vs Time
73.060
73.058
73.056
73.054
73.052
73.050
73.048
73.046
73.044
Latitude (°N, 1 NM range)
R
G
B
W
217.88
217.90
217.92
Longitude (°E, 1 NM range)

Figure 3

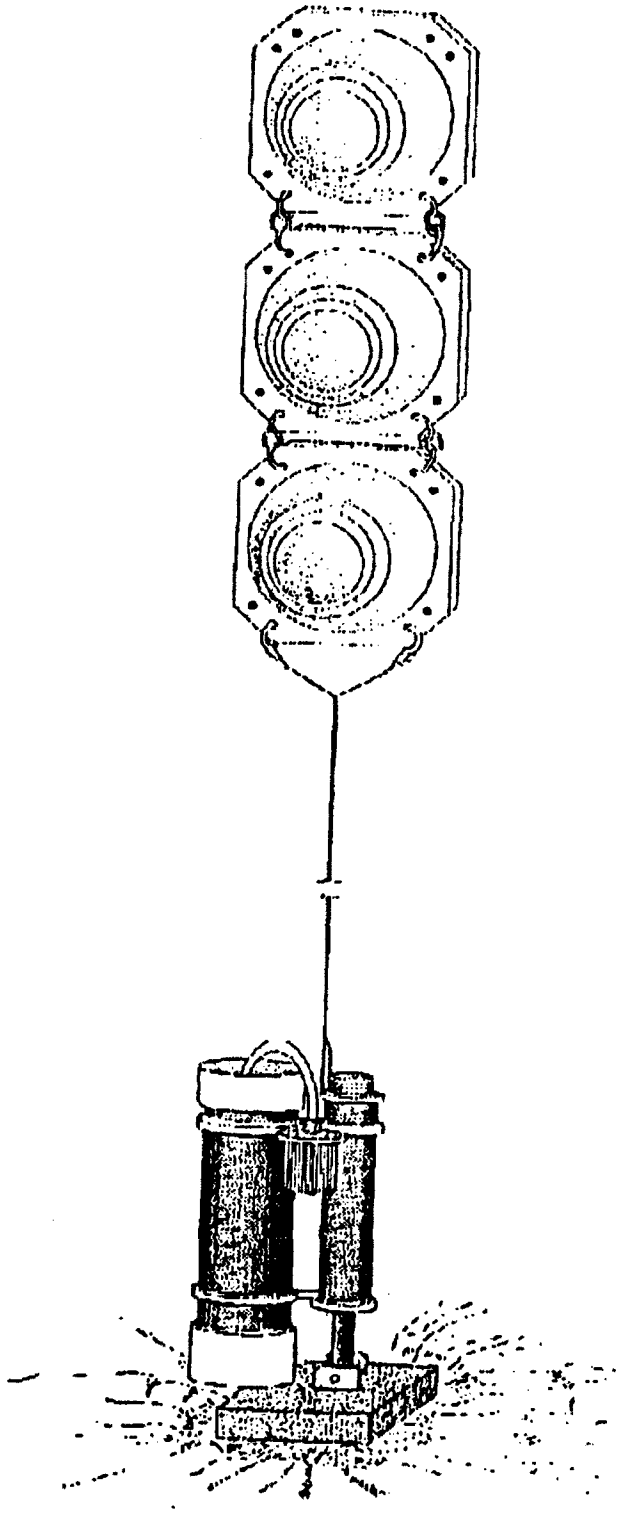

Figure 4

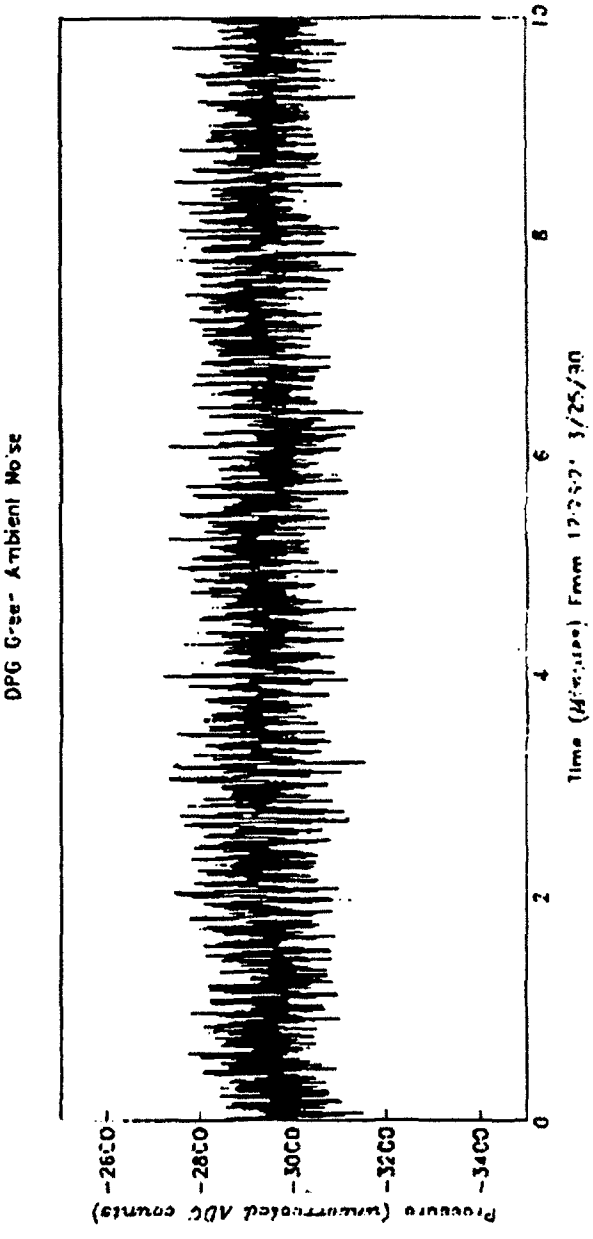

Figure 5

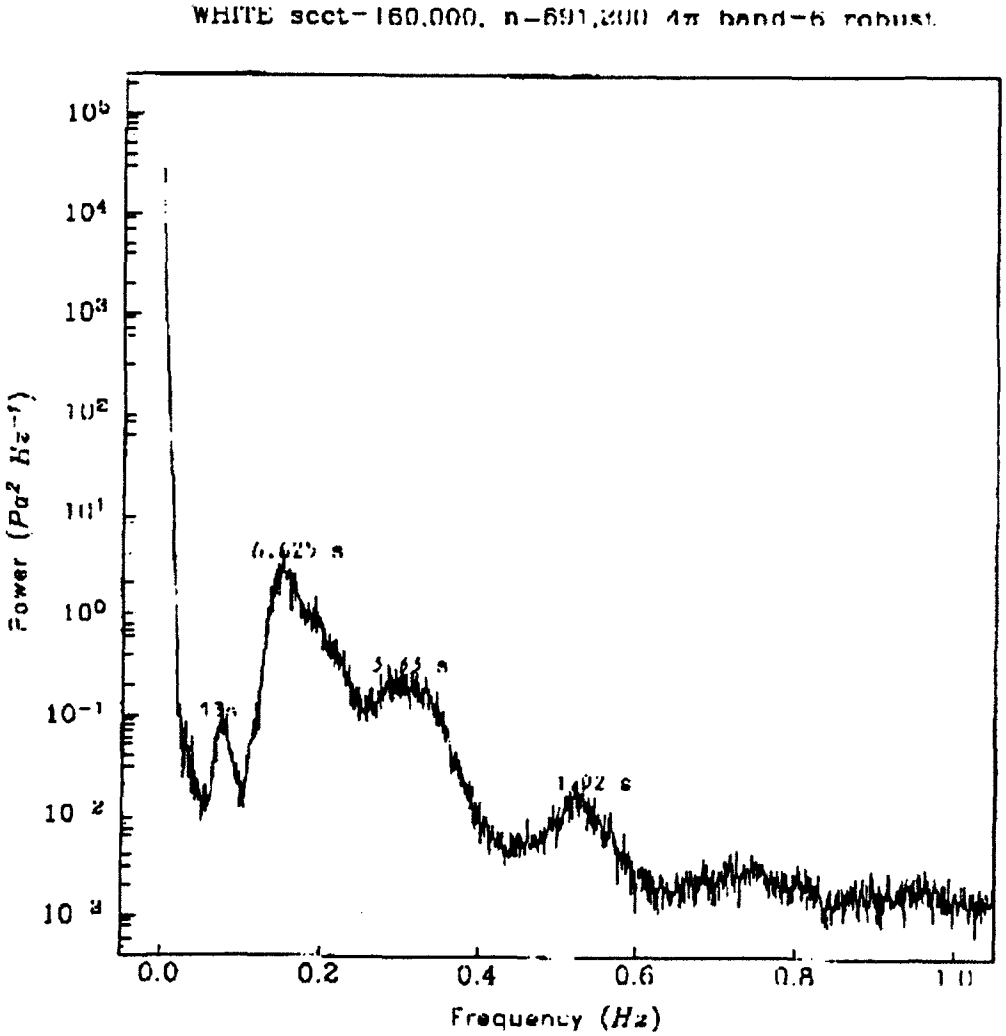
WHITE sect=160,000, n=691,200 4π band=6 robust
Power (Pa^2 Hz^{-1})
Frequency (Hz)
0.0
0.2
0.4
0.6
0.8
1.0

Figure 6

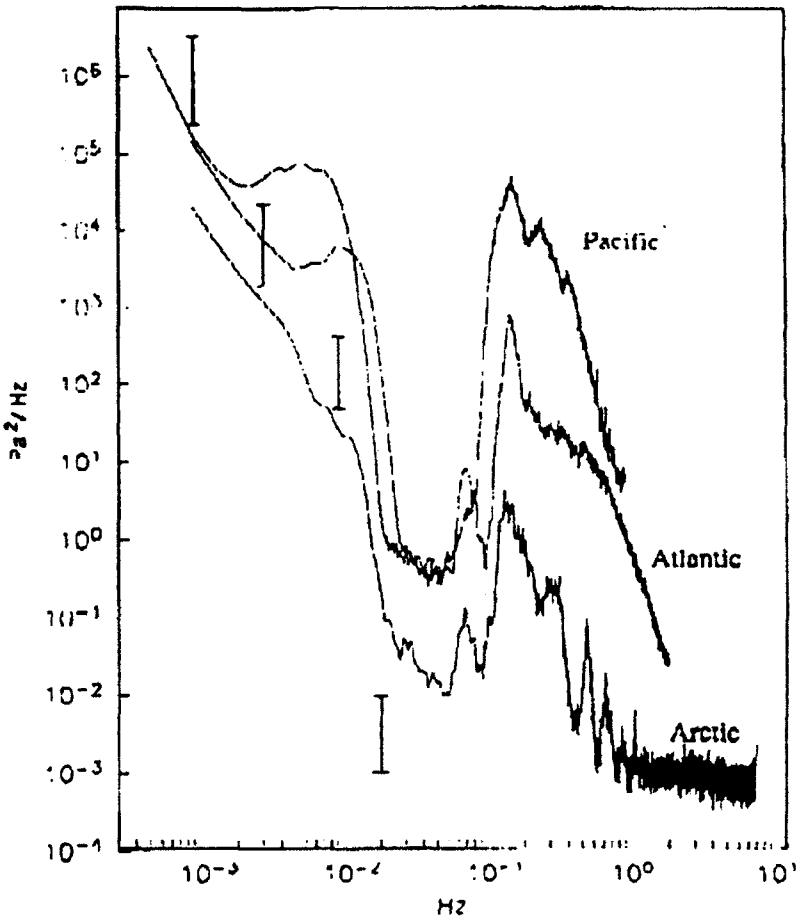

Figure 7

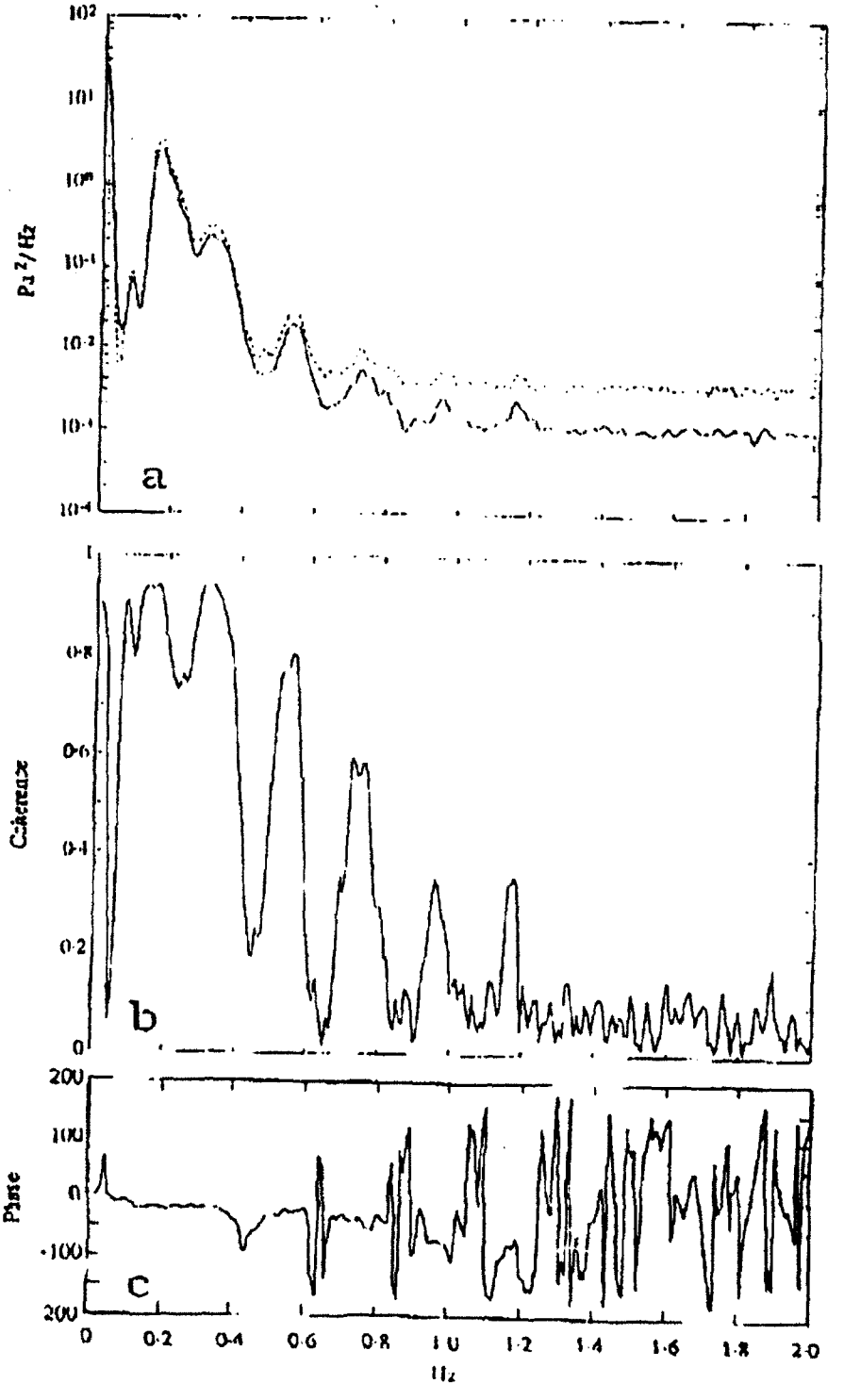

Figure 8

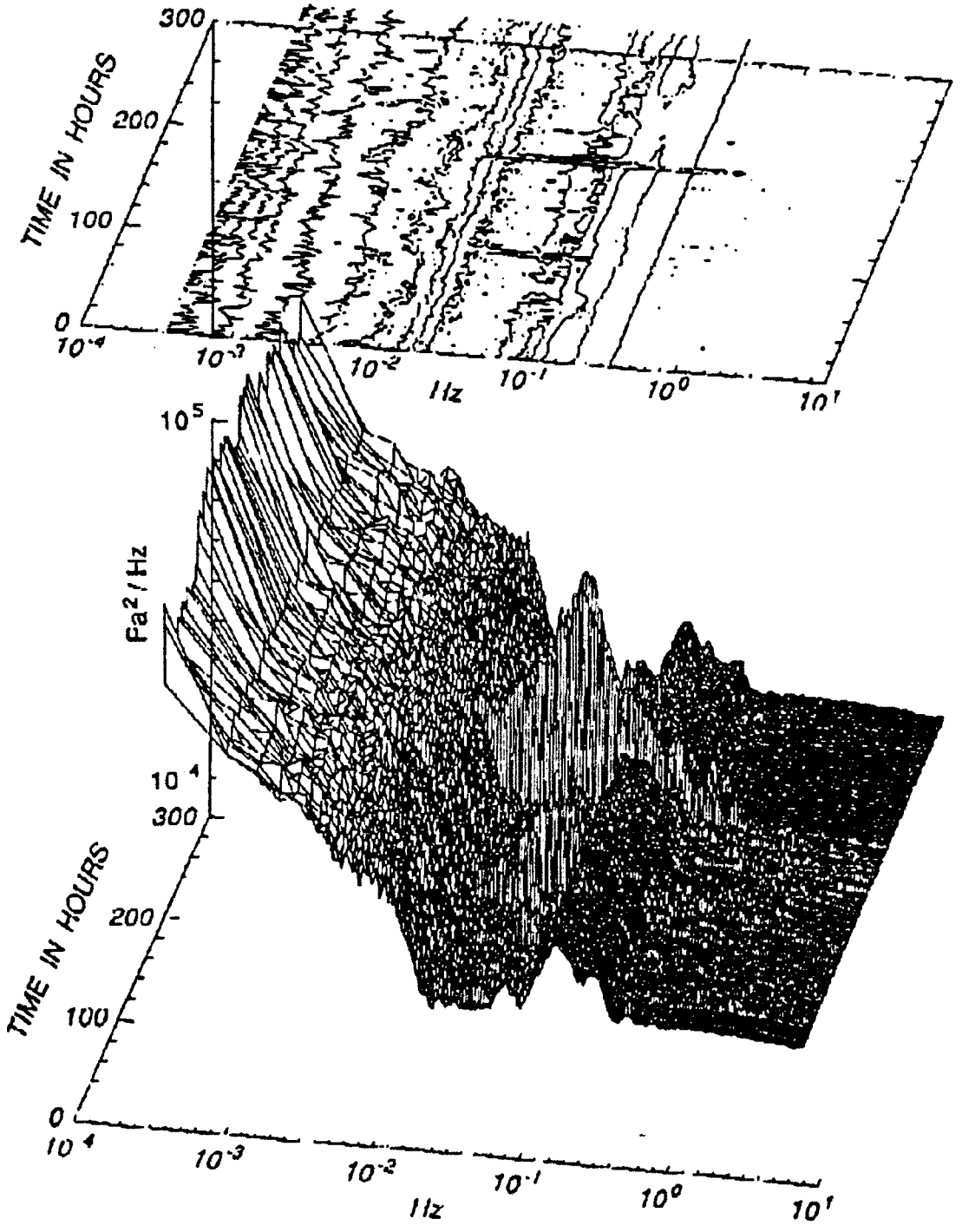
300
200
100
0
TIME IN HOURS
10^{-4}
10^{-3}
10^{-2}
10^{-1}
10^{0}
10^{1}
Hz
10^{5}
Fa^2/Hz
10^{4}
300
200
100
0
TIME IN HOURS
10^{-4}
10^{-3}
10^{-2}
10^{-1}
10^{0}
10^{1}
Hz

Figure 9

S

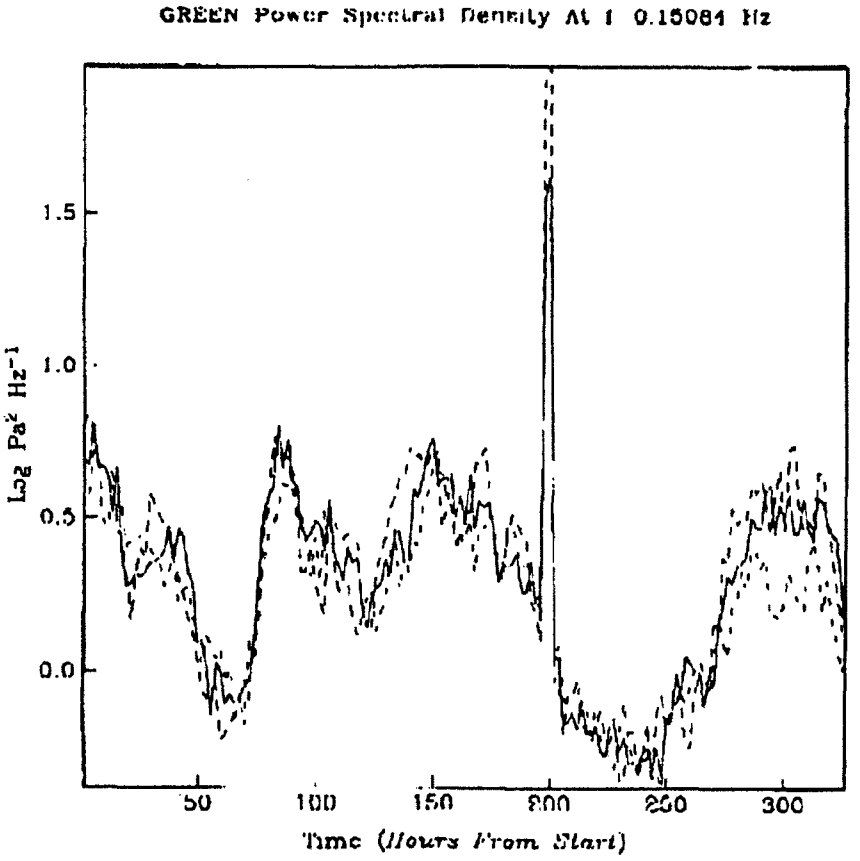
GREEN Power Spectral Density At f 0.15084 Hz
1.5
1.0
0.5
0.0
L_2 Pa^2 Hz^{-1}
50
100
150
200
250
300
Time (Hours From Start)

Figure 10

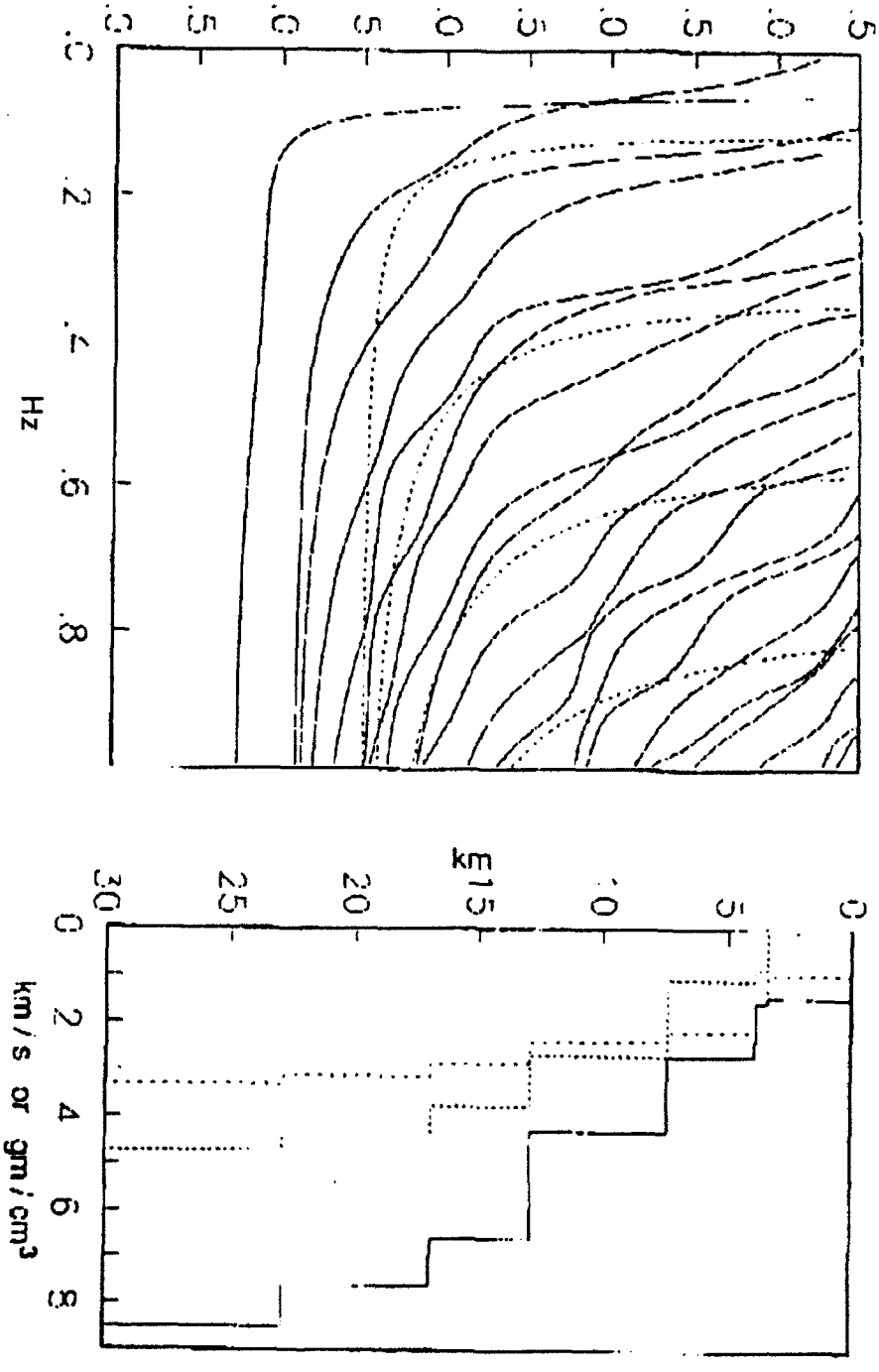

Figure 11

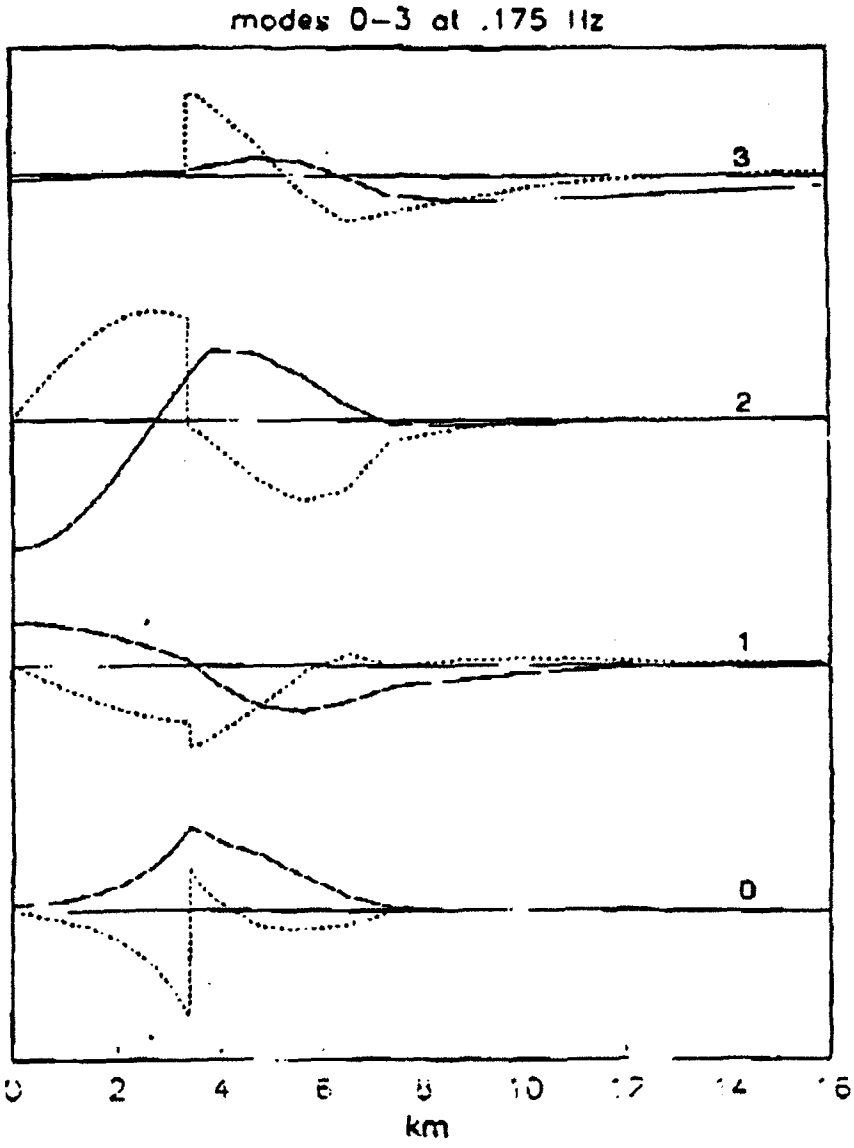

Figure 12

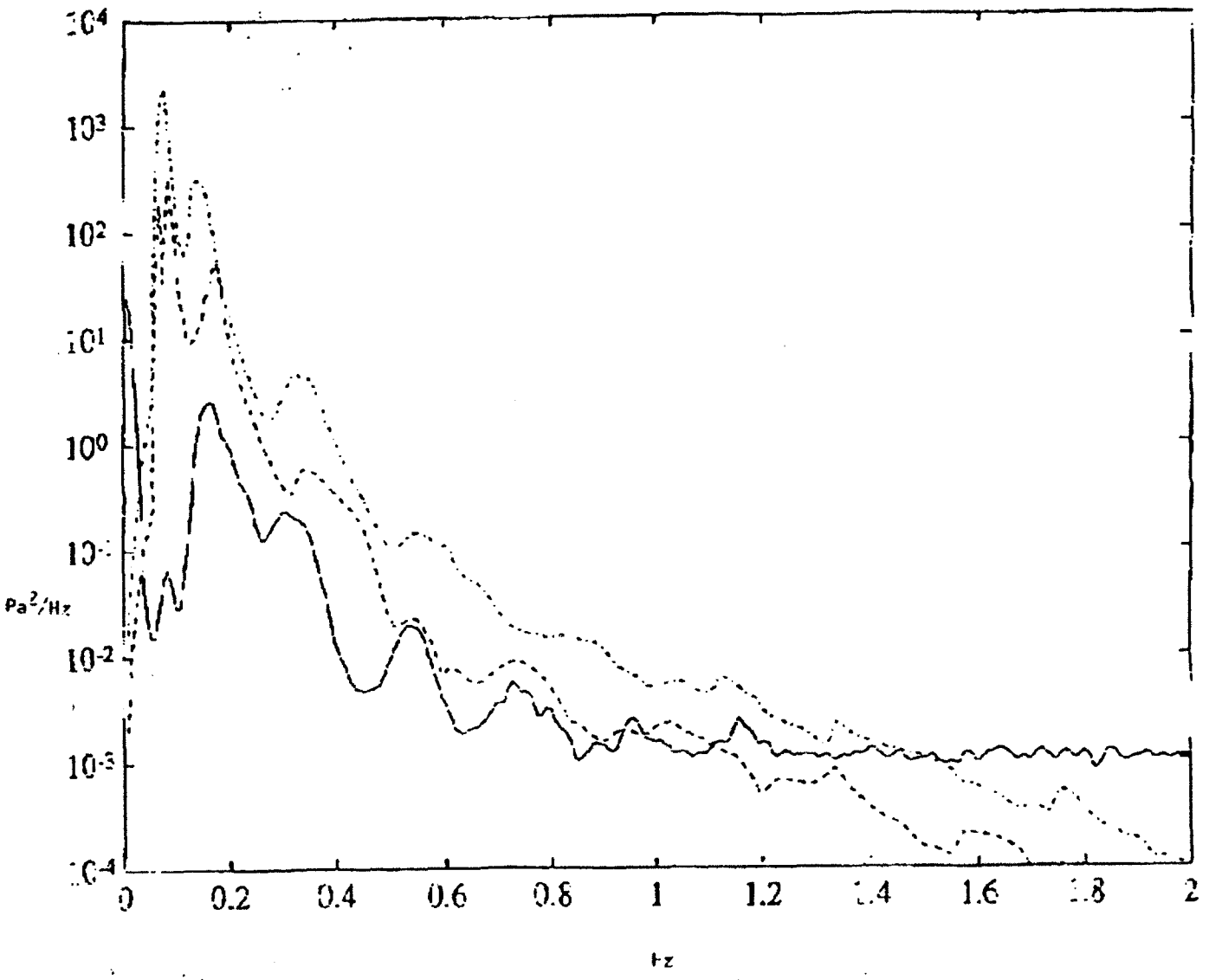
10^4
10^3
10^2
10^1
10^0
10^{-1}
10^{-2}
10^{-3}
10^{-4}
Pa^2/Hz
0
0.2
0.4
0.6
0.8
1
1.2
1.4
1.6
1.8
2
Hz

Figure 13

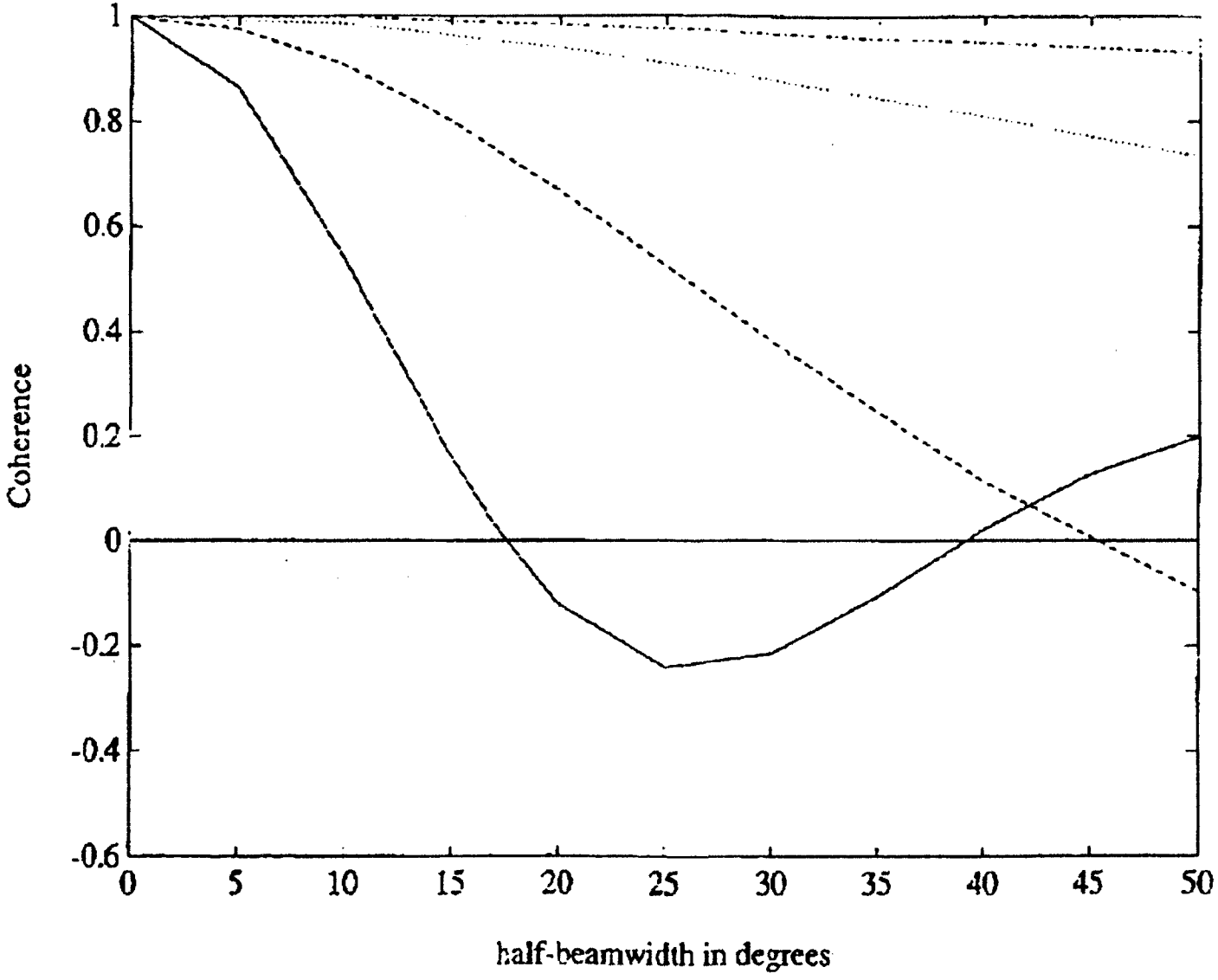
1
0.8
0.6
0.4
0.2
0
-0.2
-0.4
-0.6
Coherence
0
5
10
15
20
25
30
35
40
45
50
half-beamwidth in degrees

Figure 14

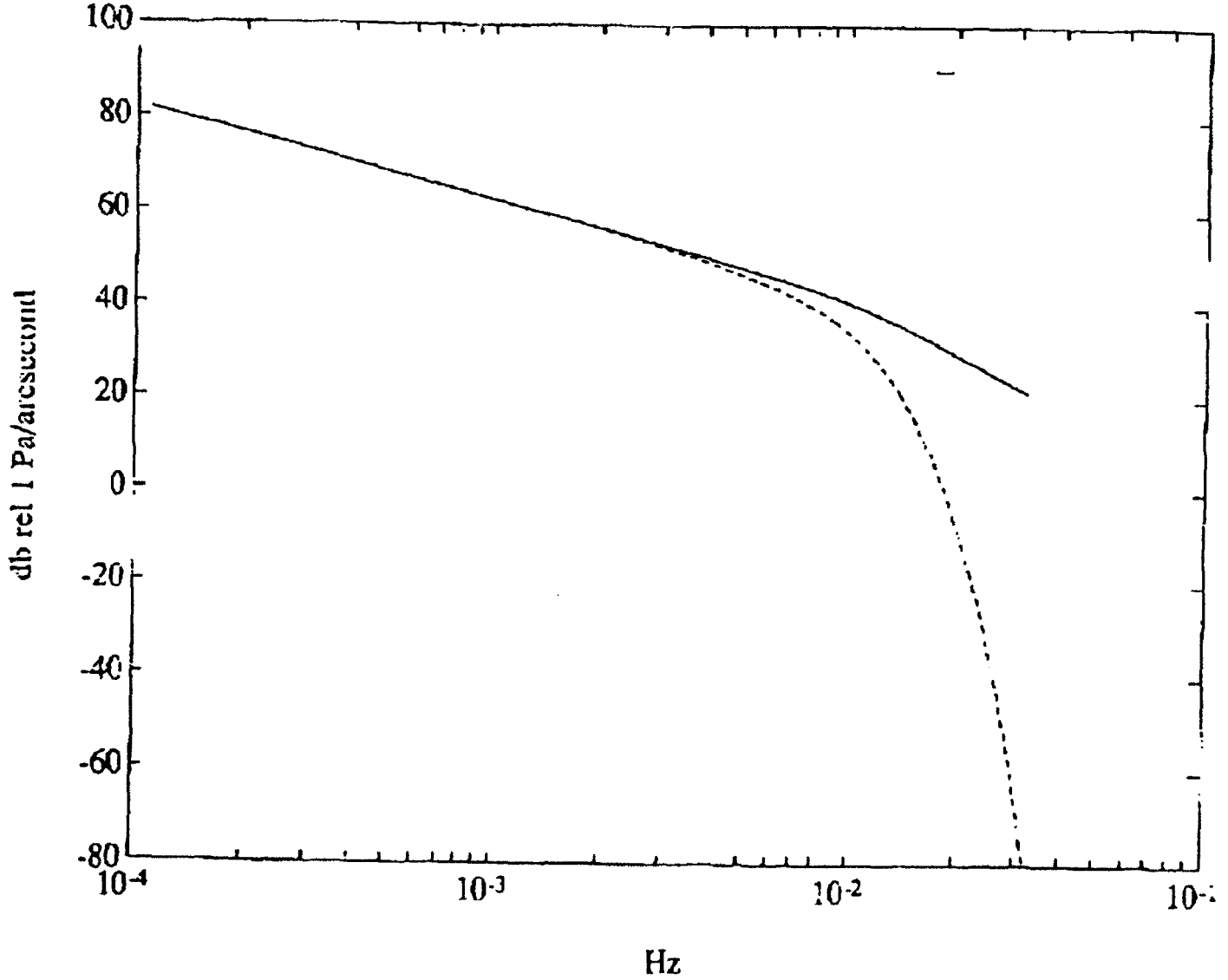

Figure 15

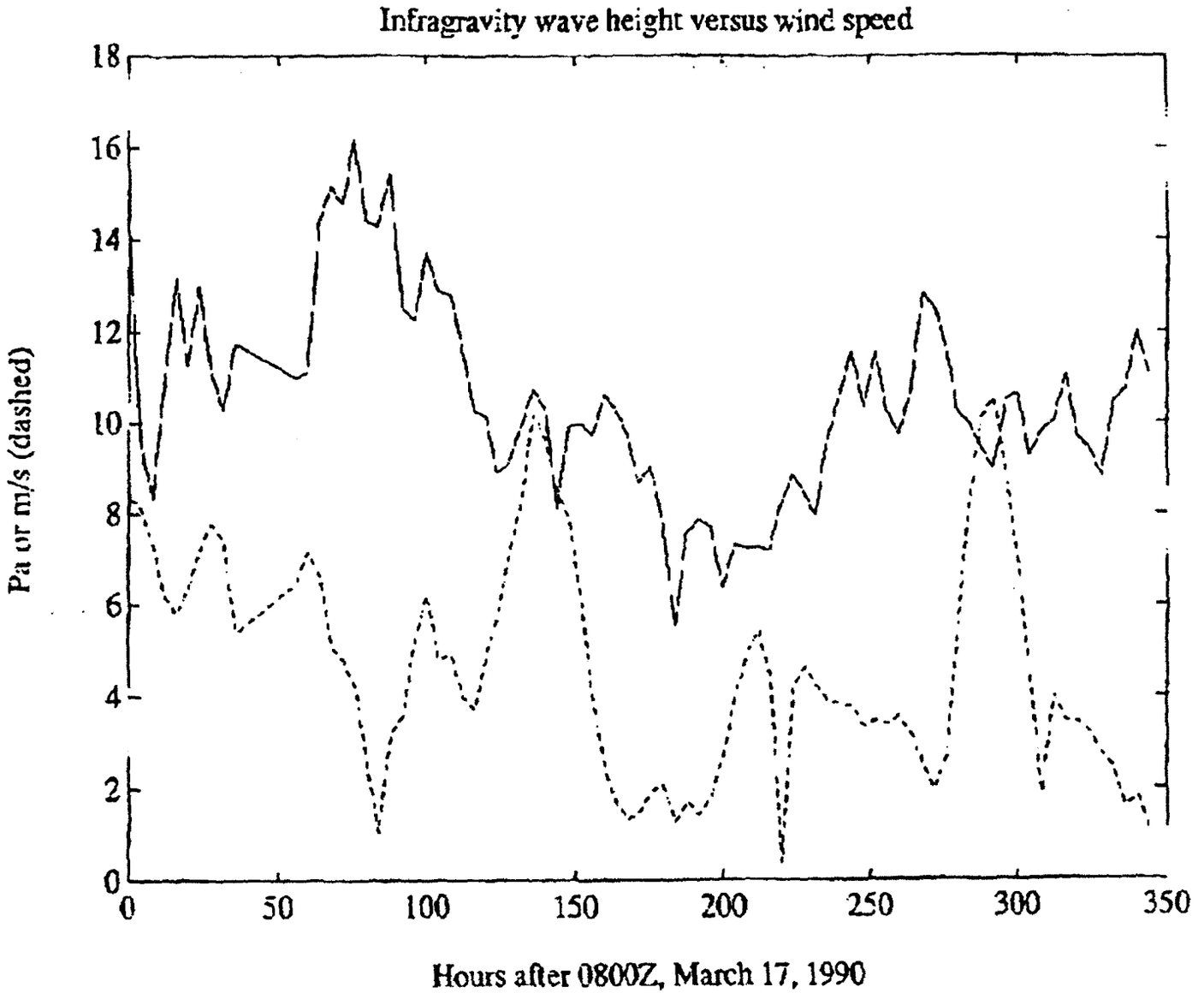
Infragravity wave height versus wind speed
Pa or m/s (dashed)
Hours after 0800Z, March 17, 1990
0
2
4
6
8
10
12
14
16
18
0
50
100
150
200
250
300
350

Figure 16

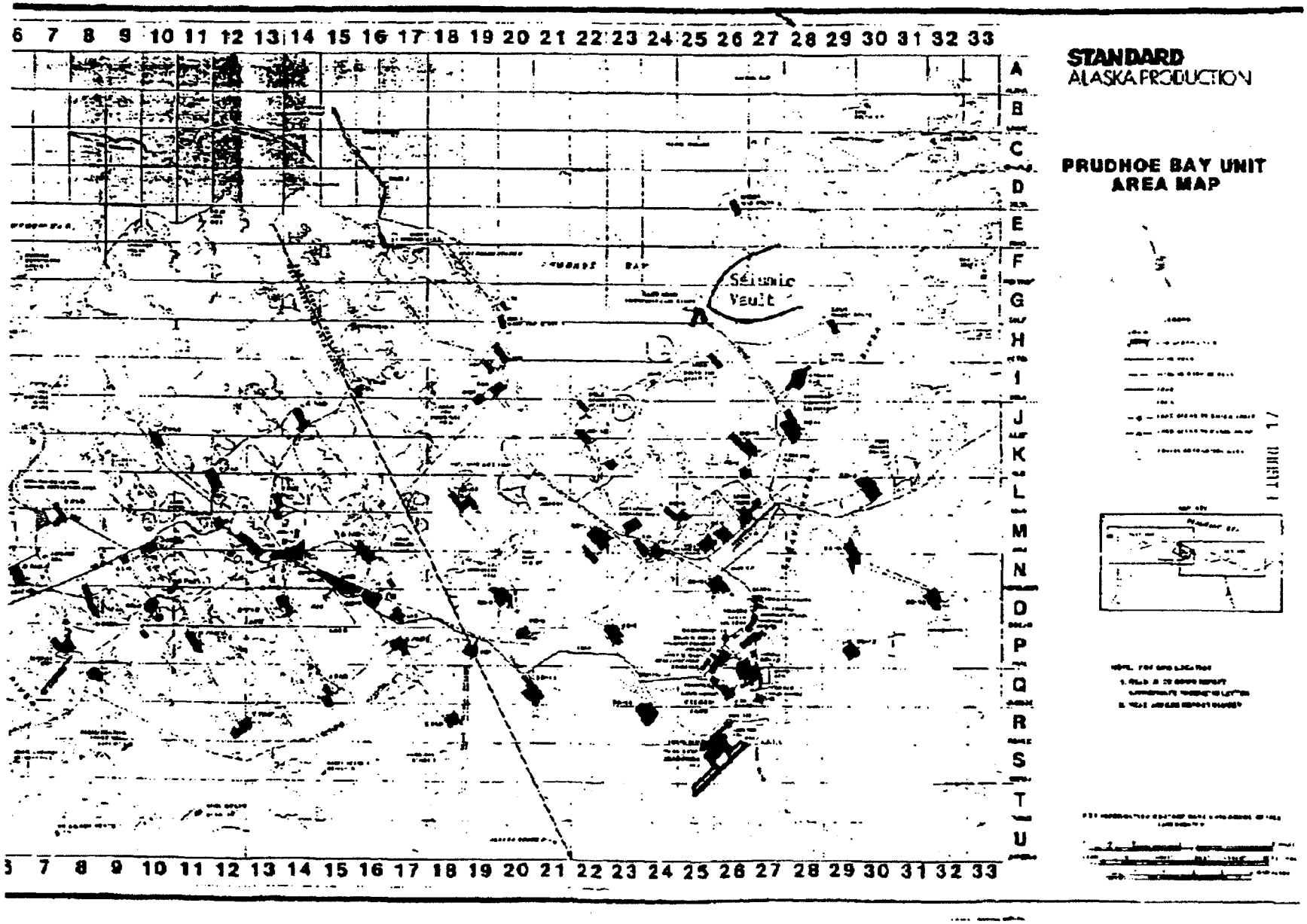
6 7 8 9 10 11 12 13 14 15 16 17 18 19 20 21 22 23 24 25 26 27 28 29 30 31 32 33
A B C D E F G H I J K L M N O P Q R S T U
Seismic Vault
STANDARD
ALASKA PRODUCTION
PRUDHOE BAY UNIT
AREA MAP

Figure 17

Figure 18

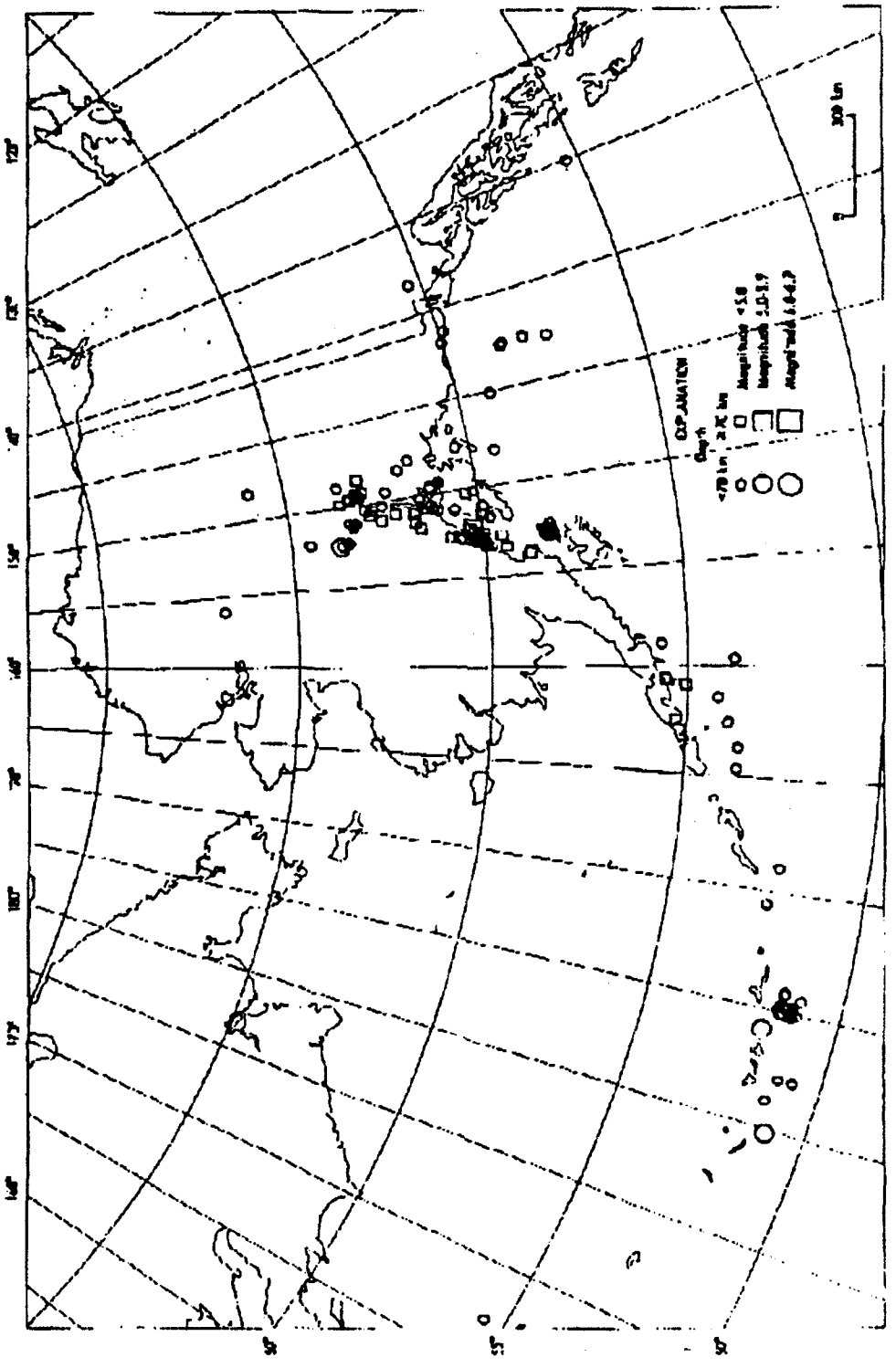
EXPLANATION
Depth
Earthquake epicenters in Alaska and adjacent regions for March, 1990 (C. Stover)

Figure 19

25 March 1990 13:22:55.60
Costa Rica

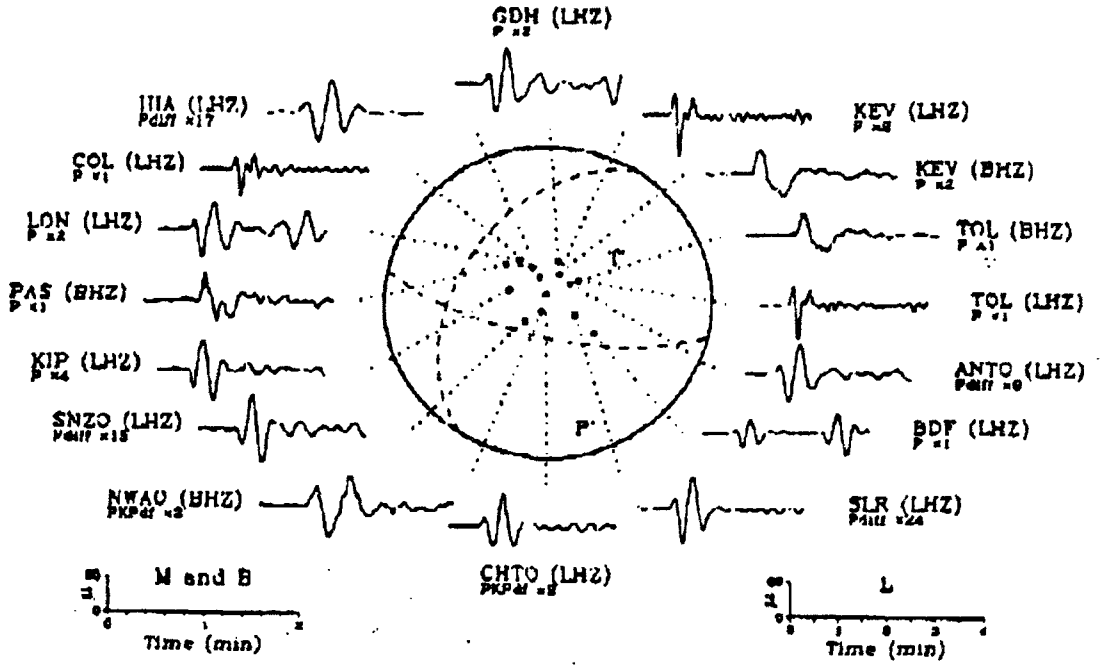

31 March 1990 19:31:42.75
Off Coast of Hokkaido, Japan

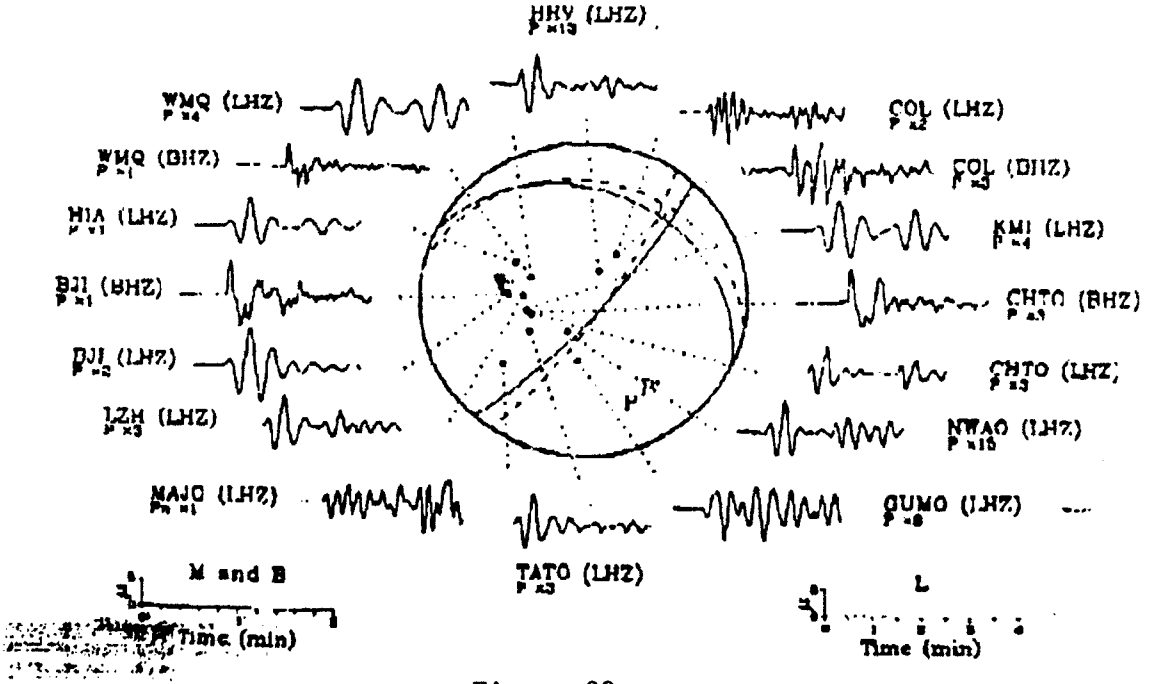

Figure 20

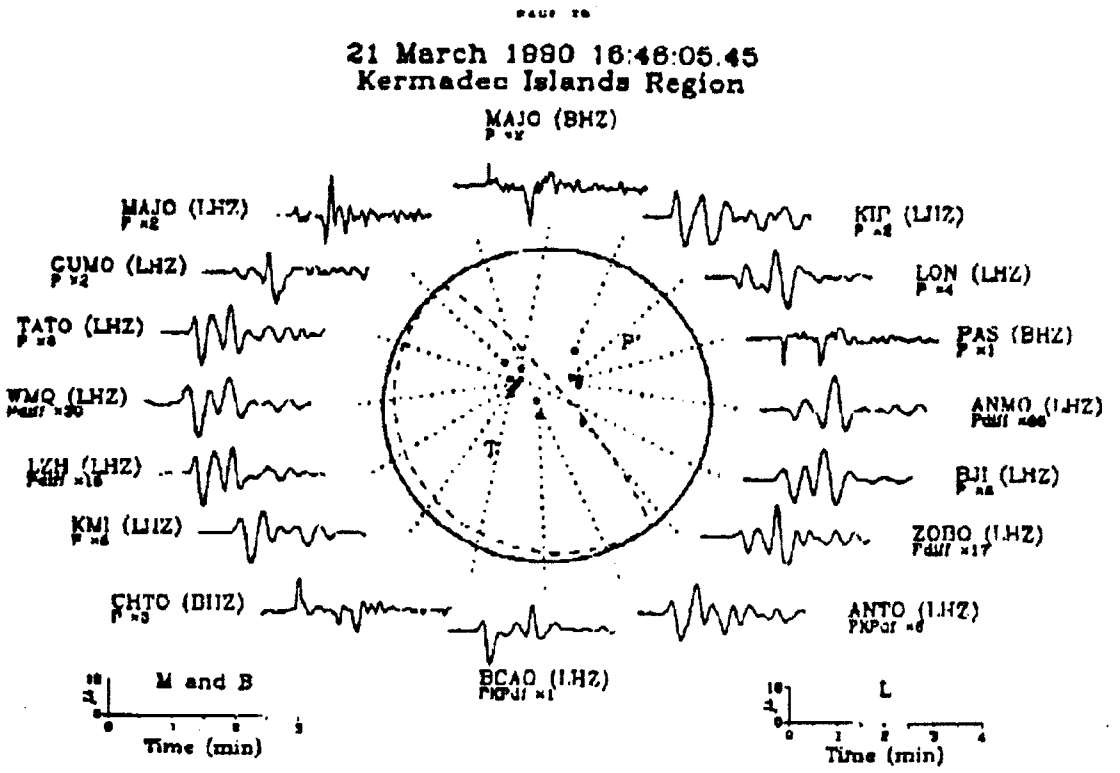
21 March 1990 16:46:05.45
Kermadec Islands Region
MAJO (BHZ)
MAJO (LHZ)
KIP (LHZ)
GUMO (LHZ)
LON (LHZ)
TATO (LHZ)
PAS (BHZ)
WMQ (LHZ)
ANMO (LHZ)
LZH (LHZ)
BJI (LHZ)
KMI (LHZ)
ZOBO (LHZ)
CHTO (BHZ)
ANTO (LHZ)
BCAO (LHZ)
M and B
L
Time (min)
Time (min)

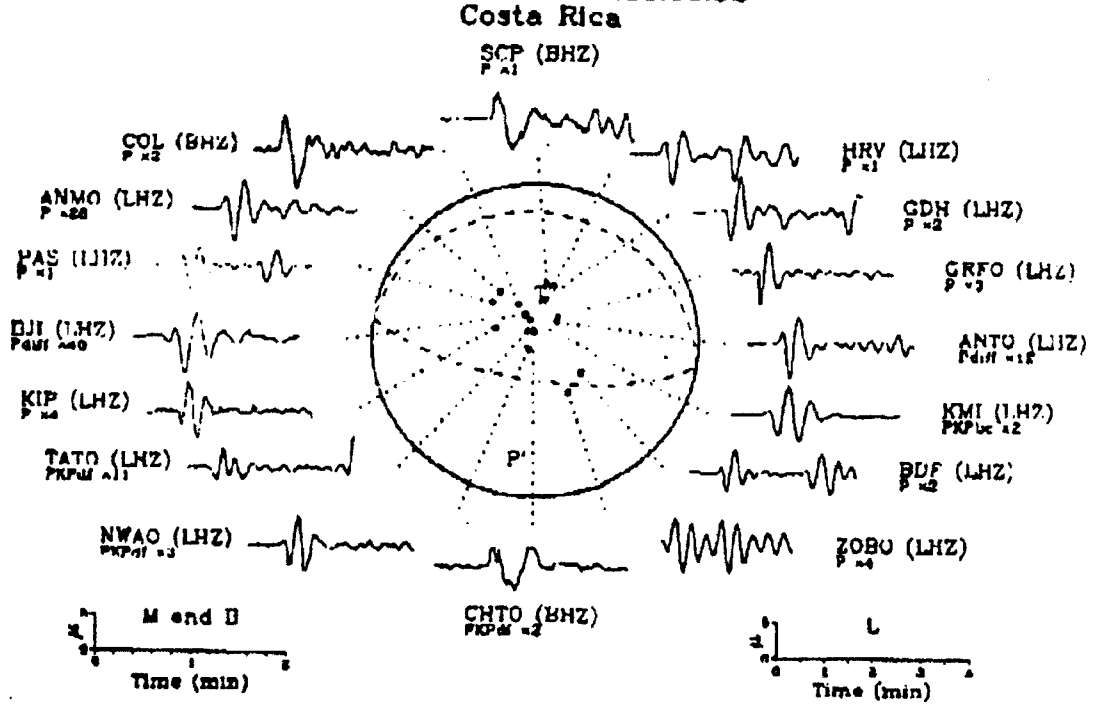
25 March 1990 13:16:06.92
Costa Rica
SCP (BHZ)
COL (BHZ)
HRV (LHZ)
ANMO (LHZ)
GDH (LHZ)
PAS (LHZ)
CRFO (LHZ)
BJI (LHZ)
ANTO (LHZ)
KIP (LHZ)
KMI (LHZ)
TATO (LHZ)
BDF (LHZ)
NWAO (LHZ)
ZOBO (LHZ)
CHTO (BHZ)
M and B
L
Time (min)
Time (min)

Figure 21

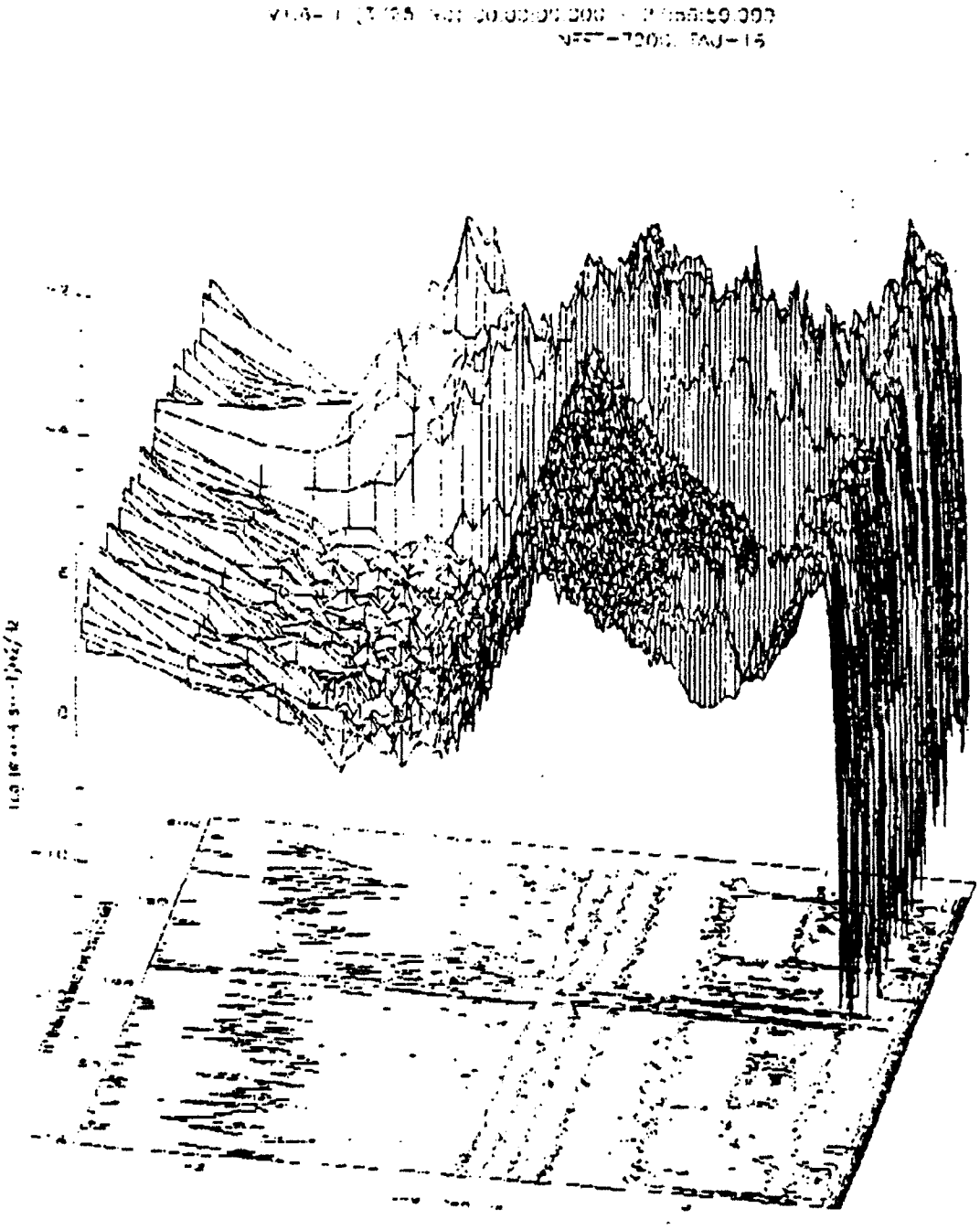

Figure 22

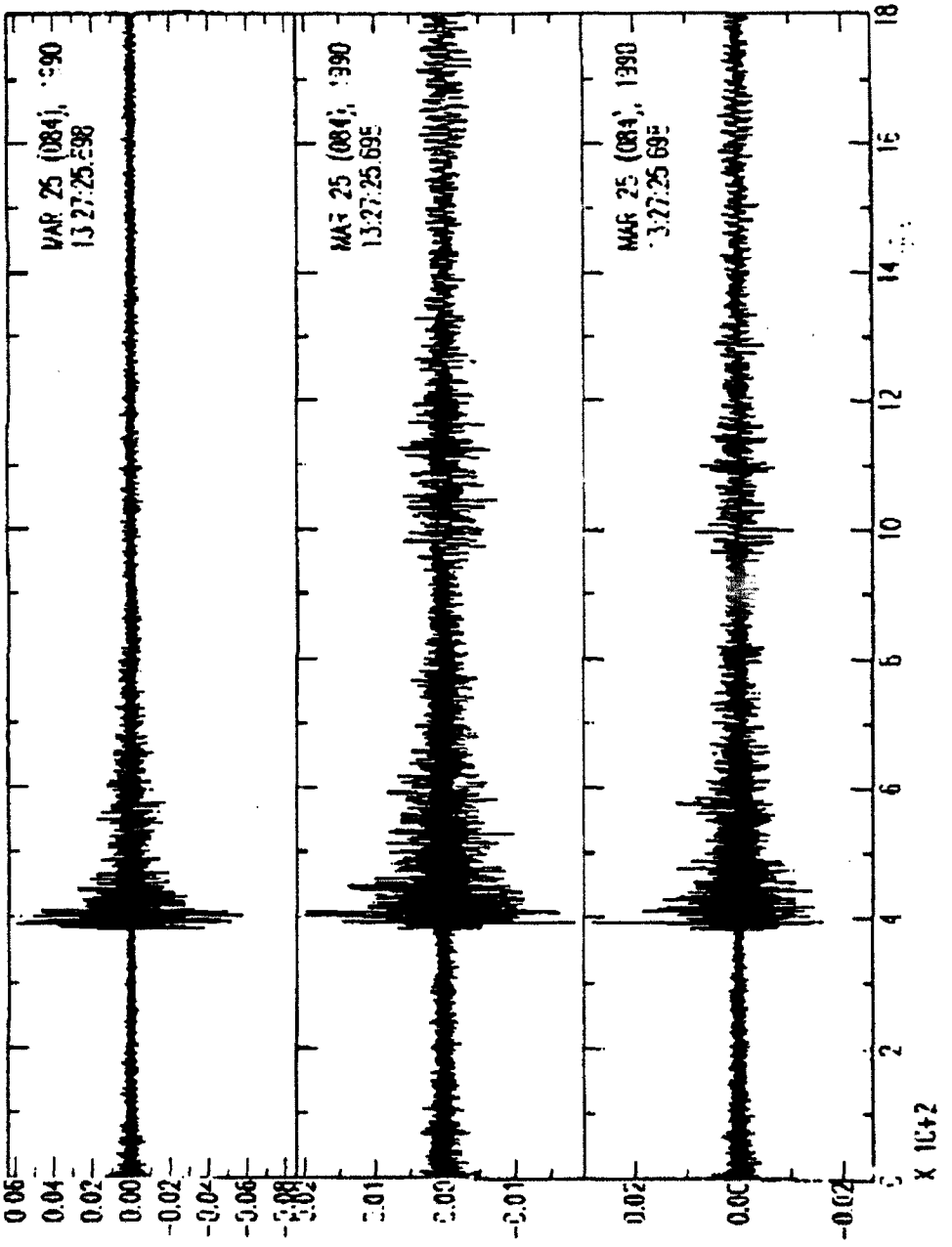
MAR 25 (084), 1990
13:27:25.598
MAR 25 (084), 1990
13:27:25.695
MAR 25 (084), 1990
13:27:25.695
0.06
0.04
0.02
0.00
-0.02
-0.04
-0.06
-0.08
0.02
0.01
0.00
-0.01
0.02
0.00
-0.02
2
4
6
8
10
12
14
16
18
X 10+2

Figure 23

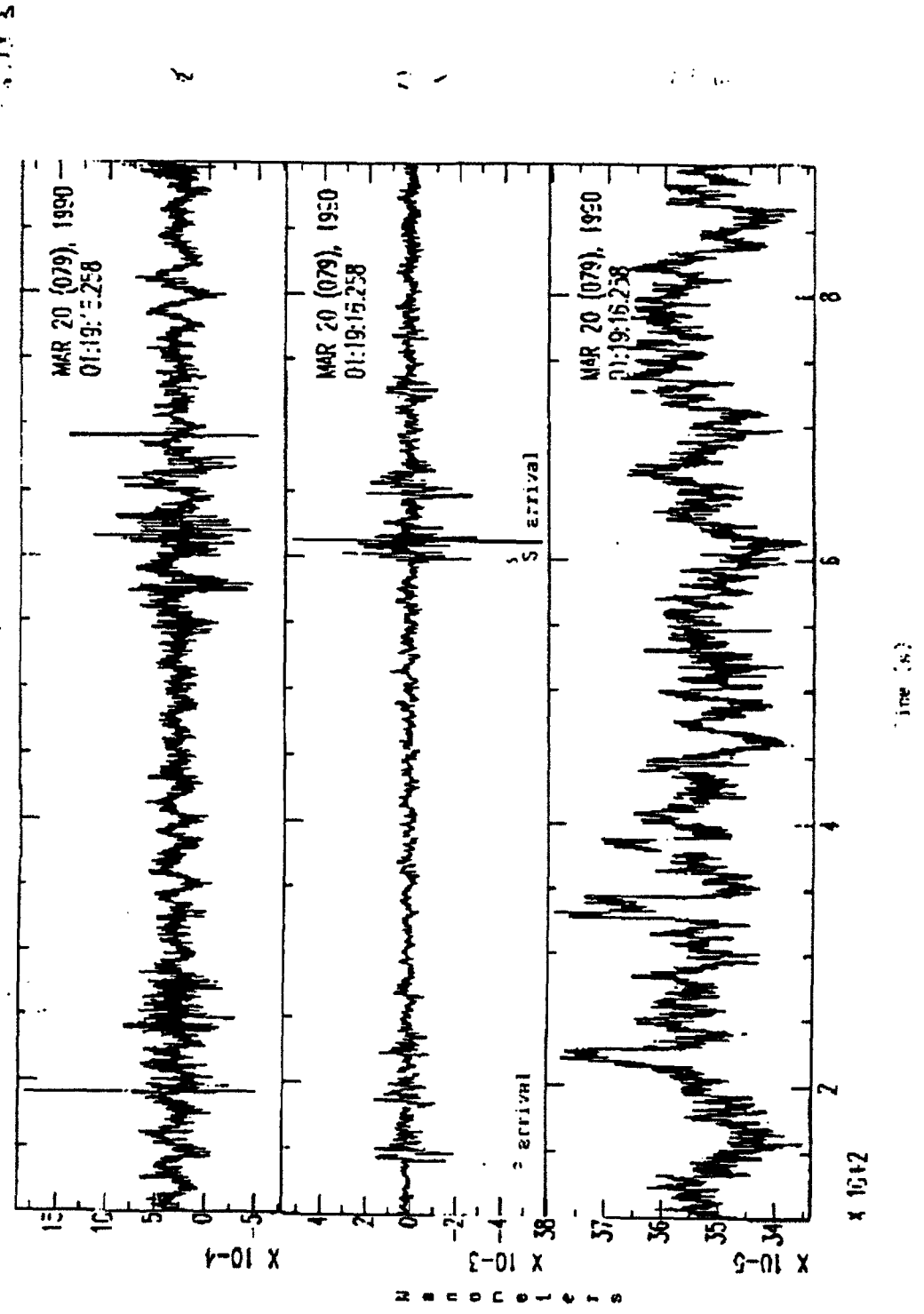
Station - Vault 3, Ice Camp
Bonin Islanc Earthquake
MAR 20 (079), 1990
MAR 20 (079), 1950
MAR 20 (079), 1950
S arrival
P arrival
X 10-4
X 10-3
X 10-5
Nanometers
x 1042

Figure 24

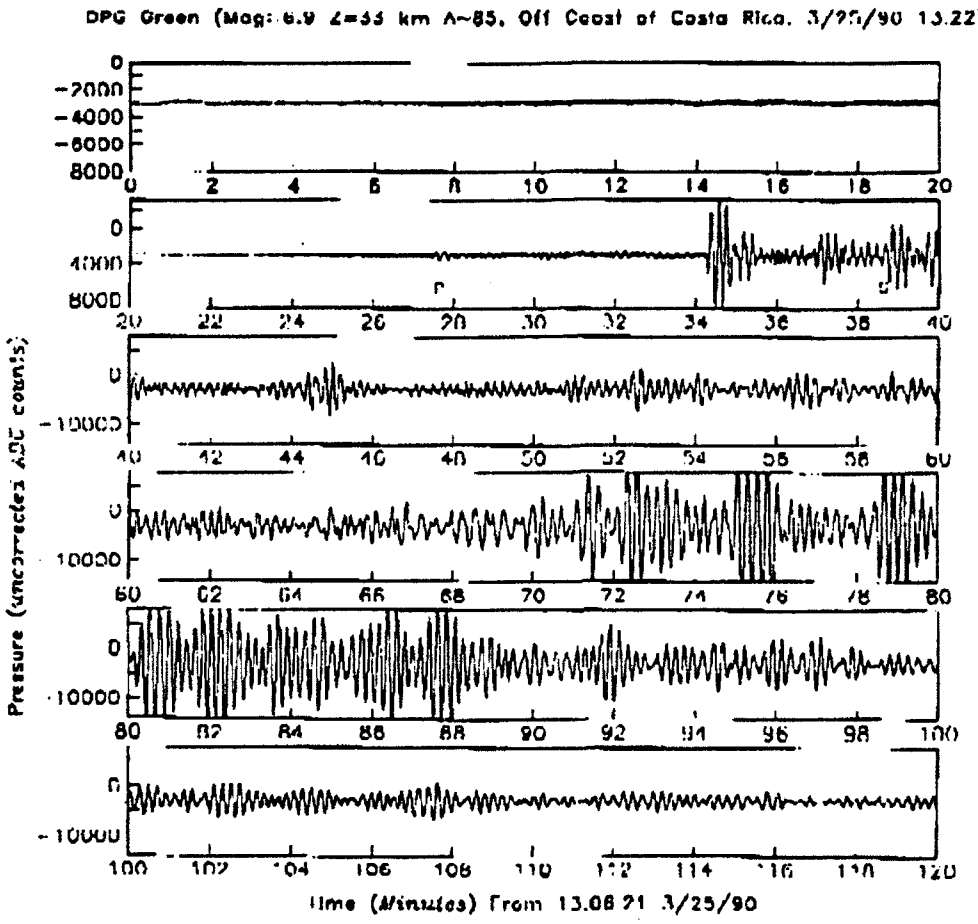
DPG Green (Mag: 6.9 Z=33 km A~85, Off Coast of Costa Rica, 3/25/90 13:22)
Pressure (uncorrected ADC counts)
Time (Minutes) From 13:08:21 3/25/90

Figure 25

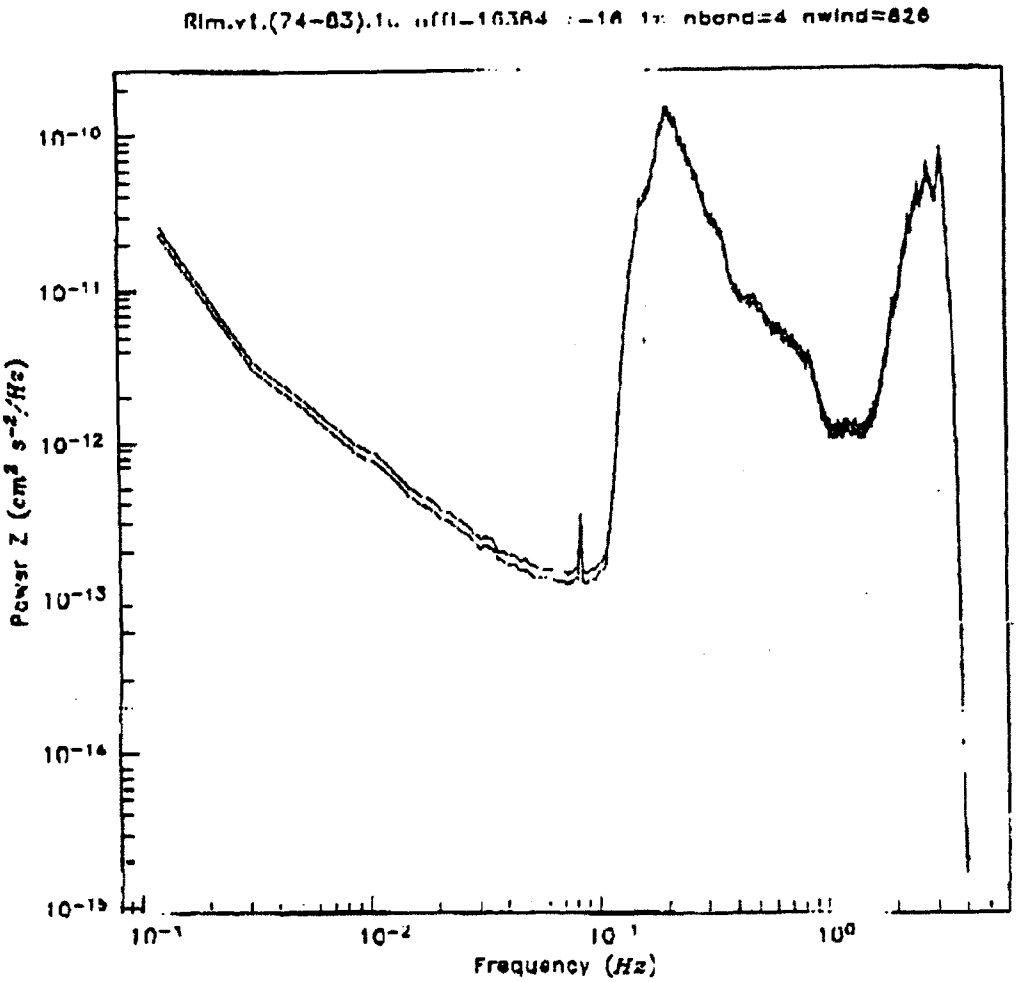
nbond=4 nwind=826
10^{-10}
10^{-11}
10^{-12}
10^{-13}
10^{-14}
10^{-15}
Power Z ($cm^2\ s^{-2}/Hz$)
10^{-1}
10^{-2}
10^{0}
Frequency (Hz)

Figure 26

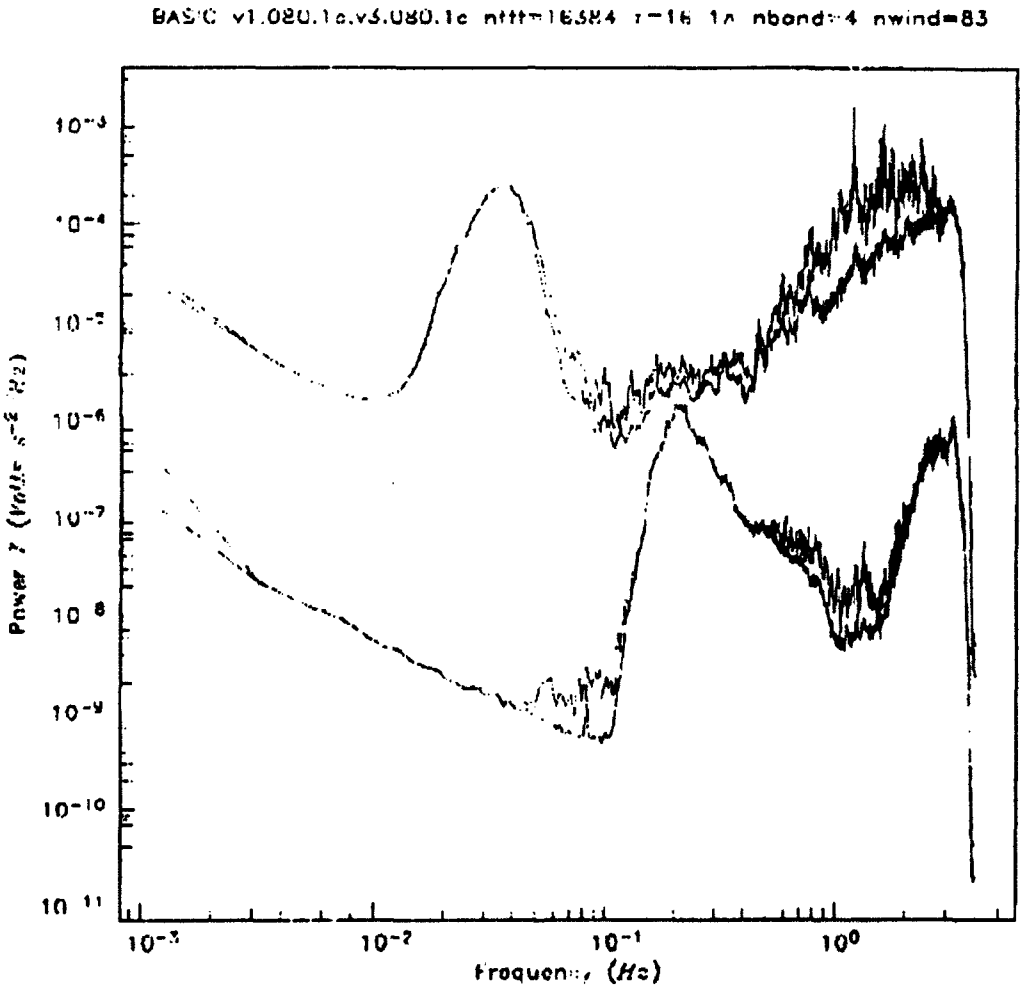
BAS'C v1.020.1c.v5.080.1c nfft=16384 r=16 1n nbond=4 nwind=83
Power ? (Volts s^-2 Hz)
10^-3
10^-4
10^-5
10^-6
10^-7
10^-8
10^-9
10^-10
10^-11
10^-3
10^-2
10^-1
10^0
Frequency (Hz)

Figure 27